MATHEMATICAL MODELING OF THE BONE REMODELING PROCESS

by

IRIS LIZETH ALVARADO

Presented to the Faculty of the Graduate School of

The University of Texas at Arlington in Partial Fulfillment

of the Requirements for the Degree of

DOCTOR OF PHILOSOPHY IN THE MATHEMATICAL SCIENCES

THE UNIVERSITY OF TEXAS AT ARLINGTON

August 2018

ACKNOWLEDGEMENTS

I would like to thank the professors that were so invested in my completion of this dissertation: Dr. Benito Chen, Dr. Gaik Ambartsoumian, Dr. Venu Varanasi, Dr. Guojun Liao, Dr. Jianzhong Su, Dr. Theresa Jorgensen, and Dr. Tuncay Aktosun. In particular, I will be forever grateful to my advisor, Dr. Hristo Kojouharov, for his great guidance and mentoring, and for always seeking the very best for his students.

I am grateful for the support system provided by the faculty, staff, and graduate students in the Mathematics Department at UTA. I have learned so much from everyone, and will always cherish my time here.

I wish to thank my loving and supportive husband, Juventino, and my daughter Olivia who provided unending motivation to complete this great journey. I am grateful to my parents, mother-in-law, and siblings for their constant encouragement.

My completion of the PhD program would not have been possible without the financial support of the Summer Dissertation Fellowship, the GAANN Fellowship, MAVS Bridge Fellowship, and the NSF GK-12 MAVS Fellowship.

A.M.D.G.

July 11, 2018

ABSTRACT

MATHEMATICAL MODELING OF THE BONE REMODELING PROCESS

IRIS LIZETH ALVARADO, Ph.D.

The University of Texas at Arlington, 2018

Supervising Professor: Dr. Hristo Kojouharov

The skeleton is a very important organ that needs to be continuously remodeled due to microdamage, changes in mechanical loading, or mineral homeostasis. The bone remodeling process is responsible for maintaining the structure and function of the skeletal system. Accumulation of microdamage that goes unrepaired within the bone matrix can lead to bone fragility and loss of mechanical properties. Evidence suggests that when microdamage is present in the bone structure, osteocyte apoptosis plays an important role in the initiation of the bone remodeling process. Osteocytes are known to release RANKL a promoter of osteoclastogenesis (bone-resorbing cells) and scelorstion an inhibitor of osteoblastogenesis (bone-forming cells).

The mathematical model presented in this work studies the initiation and organization of cells within a cortical bone multicellular unit (BMU) in the presence of microdamage. We did this by extending a base model and incorporating the role of osteocytes and a signaling pathway known to regulate bone formation Wnt canonical pathway. Equilibrium and stability analysis was performed on several simplifications of the model that indicated that osteocytes may reach their maximum density depending on the rate at which osteoblast cells undergo apoptosis or become embedded

in the bone matrix. Numerical simulations were performed using MATLAB in which we study the initiation of the process in the presence of several sized microcracks. Additionally, we study age-related bone disorders and potential therapeutic targets to overcome such disorders.

TABLE OF CONTENTS

LIST OF ILLUSTRATIONS

LIST OF TABLES

1 Introduction

The skeletal system has several important functions such as structural support, protection of vital organs, movement, and mineral storage. In order to carry out these functions, bones need continuous replacement and maintenance. The process in which mature bones are continuously replaced throughout our lifetime is termed bone remodeling. Bones need to be able to withstand and account for everyday changes mechanical loading and accumulation of microdamage within the bone matrix [27, 4]. Microdamage that goes unrepaired can lead to bone fragility and loss of mechanical properties [43]. The bone remodeling process is therefore responsible for repairing microdamage and keeping the optimal structure of the skeletal system. This is done through the tight coupling of resorption and formation bone. Imbalances between bone resorption and bone formation can lead to several bone diseases such as osteoporosis, Paget's disease, and osteopetrosis [13]. Bone diseases can arise in both men and women for a variety of factors such as hormonal and age-related changes; e.g. about 10 million Americans over the age of 50 have osteoporosis and approximately 1 million have Paget's disease [13]. Mathematical modeling of biological processes such as bone remodeling has proven useful in better understanding these processes, explaining diseases, and developing potential therapies [36].

1.1 Bone Cells

Removal of old bone and formation of new bone are done by two main bone cells: osteoclasts and osteoblasts, respectively. Osteoclast cells are derived from hematopoietic stem cells and osteoblast cells are derived from multipotent mesenchymal stem cells [27]. Both types of stem cells go through several commitment and differentiation stages before becoming active cells that remove or form bone. Once they have

completed their lifespan, osteoblast and osteoclast undergo apoptosis. Osteoblasts, however, have two alternative fates; they can become bone lining, quiescent, cells which are found on the surface of bone, or they can become embedded in the bone matrix and differentiate further into osteocyte cells [4].

Extensive research has been done over the importance of the osteoblast and osteoclast cells and their role in the bone remodeling process, however, there has been increasing evidence that osteocytes have an equally important role in bone remodeling. Osteocytes are the most abundant cell type in bone making up over 90% of all bone cells in the adult skeleton [6]; they are formed when approximately 5 to 20% of osteoblasts are buried in the osteoid they are forming [4]. Osteocytes live within structures called lacunae and are extensively connected to one another through their cytoplasmic extensions. Osteocyte density within the bone matrix has been studied as an indicator of age or disease; several papers have linked osteocyte cell density with age and bone diseases in humans and rats [29, 24, 45, 16]. Authors in [29] presented decreasing linear correlations between osteocyte density and age. Additionally, authors in [44] suggest that osteocyte cells, rather than the work done by osteoclasts and osteoblasts, determines bone mass and volume. Due to the osteocytes' optimal location within the bone matrix and their extensive network, they are thought to sense microdamage in bone or changes in mechanical loading that initiate bone remodeling [4]. Osteocyte apoptosis occurs through the accumulation of microdamage in the skeletal system when the microdamage interferes with the osteocyte connections [17, 42]. Osteocyte apoptosis has also been shown to occur through unloading or excessive loading of bones [30, 17], where excessive overloading is always followed by osteoclast recruitment and resorption.

1.2 Signaling Pathways and other Key Factors

Several important signaling pathways and factors that regulate the proliferation, differentiation, and apoptosis of bone cells in the bone remodeling process have been identified in literature. In this section we will focus on those we believe are the key players in this complex biological process. These include growth factors, signaling ligand-receptor pathways, and systemic hormones.

Transforming growth factor-beta (TGF-β) has many roles in bone homeostasis, bone cancers, and metastases [18]. One of its main roles in the bone remodeling process is to balance bone formation and bone resorption. Active osteoclasts have been shown to activate TGF-β and other similar growth factors, found within the bone matrix, through the resorption of bone [5]. The release of TGF-β then increases differentiation in the early stages of osteoblastogenesis, but blocks further differentiation into the active osteoblast cells along with bone mineralization. Furthermore, TGF-β has been shown to induce osteoclast differentiation and apoptosis [15].

One signaling pathway that has been studied for about two decades because of its importance in the regulation of osteoclastogenesis is the RANK-RANKL-OPG pathway [37]. The receptor-activator nuclear factor $\kappa\beta$ (RANK) is expressed on the surface of osteoclast precursor cells. Cells in the osteoblastic lineage are known to produce the surface-bound ligand, RANKL, and the soluble decoy receptor osteoprotegerin, OPG [37]. Cell-cell binding of RANK and RANKL promotes the differentiation of osteoclast precursors, and OPG acts as an inhibitor by binding to RANKL (see Figure 1). Recent discoveries have been made about the osteocytes' role in the pathway. The osteocytes are able to express a soluble form of RANKL and promote osteoclastogenesis [46]. The authors in [46] also suggested there is an increase in RANKL production when osteocyte apoptosis occurs; i.e. RANKL is produced when there are changes in mechanical loads or microdamage is present. Others have suggested

that osteocyte apoptsosis initiates targeted bone remodeling through this elevated production in RANKL and recruitment of osteoclasts [12, 19].

A less well-known signaling pathway is the Wnt canonical pathway which has been identified as a regulator of osteoblastogenesis [23]. Wnt canonical signaling is initiated by secreted Wnt ligands binding to the co-receptors low-density lipoprotein receptor-related protein, LRP, and Frizzled. Through this extracellular binding, there is no degradation of the intracellular signaling mediator β-catenin which then accumulates in the cytoplasm and translocates to the nucleus where it controls target gene transcription [3, 20]. This signaling pathway is known for regulating commitment to the osteoblastic lineage as well as for osteoblastic precursor proliferation and differentiation (see Figure 2). Osteocytes have been shown to secrete an inhibitor of the pathway, sclerostin, which binds to LRP preventing signaling [4].

Systemic hormones, such as glucocorticoids, estrogen, parathyroid hormone (PTH) and vitamin D, have been shown to regulate the differentiation and apoptosis rates of bone cells [26]. PTH has been studied due to its importance in regulating bone remodeling and because of its involvement in clinical trials as a therapy for treating low bone mass in osteoporosis. PTH has been shown to bind to its receptor on the surface of cells in the osteoblastic lineage, including osteocytes, to promote the production of RANKL and increase bone resorption [47].

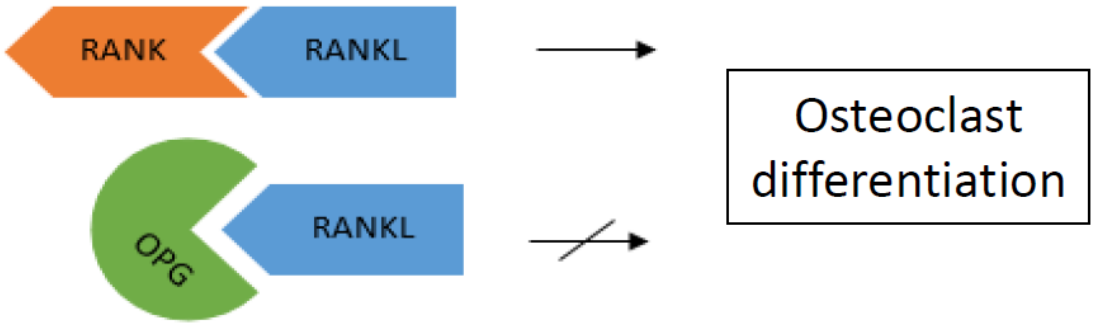

Figure 1. Schematic of the ligand, receptor, and inhibitor interaction in the RANK-RANKL-OPG Pathway - a regulator of osteoclastogenesis..

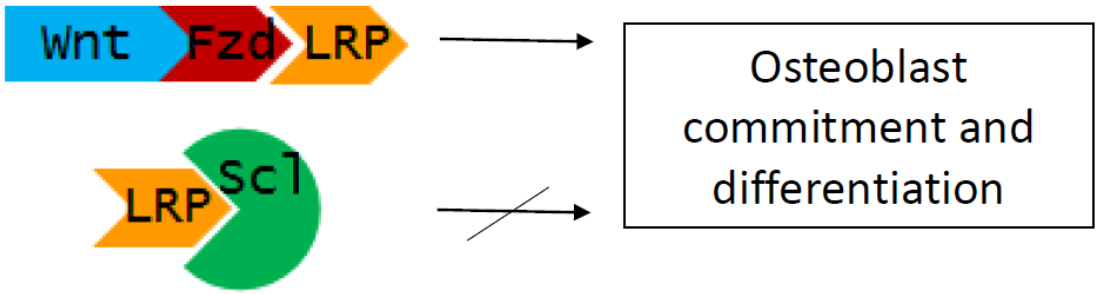

Figure 2. Schematic of the ligand, co-receptors, and inhibitor interaction in the Wnt Canonical Pathway - a regulator of osteoblastogenesis..

1.3 Bone Structure

Due to its complexity, bone can be described at various length scales; at the macroscale we can distinguish between cancellous (spongy) or cortical (compact) bone. Although cancellous bone is more metabolically active [39], cortical bone comprises 80% of all skeletal mass [38]. Additionally, cortical bone is known to bear

much of mechanical loads and is subject to fatigue damage [35, 34]. Bone remodeling that is site-specific such as that initiated by the presence of microdamage is termed targeted bone remodeling.Cortical bone at the microscale is composed mostly of cylindrically-shaped osteons in which sheets of mineralized collagen (lamellae) fibers wrap in concentric fashion around a Harvesian canal. Within the canal is a capillary for the osteon, which provides blood and nutrients to the surrounding bone matrix [39]. Additionally, the stem cells necessary for executing the bone remodeling process are thought to travel to the remodeling site via the capillary [34].

1.4 Bone Multicellular Unit (BMU)

The bone remodeling process is executed by a unit of organized cells called the bone multicellular unit, BMU, composed of cells in the osteoclastic (bone-resorbing) and osteoblastic (bone-forming) lineages. The active osteoclasts and osteoblasts and their precursor cells are able to remove old bone and form and deposit new bone restoring it to its healthy state. The BMU organization varies only slightly among the types of bone, cortical (compact) and trabecular (spongy). For cortical bone, precursor cells and nutrients are supplied to the BMU through a small capillary, called the Harvesian canal, that grows along with the BMU [39]. At the front of the BMU, the resorption zone, active osteoclasts lead the bone turnover by breaking down and resorbing the bone matrix. At the end of the BMU, the formation zone, active osteoblasts refill the cavity with osteoid which then becomes mineralized.

1.5 Types of Microdamage found in Bone

Arguably, the main purpose of the bone remodeling process is to prevent accumulation of microdamage [27, 28, 2] that occurs due to everyday loading conditions.

Bone remodeling termed as targeted is site-specific to mechanical changes or microdamage. There are two main types of microdamage that occur in bone: linear microcracks and diffuse damage. Although both affect the integrity of the skeletal system, linear microcracks, which mostly occur in interstitial bone, are known to initiate the bone remodeling process, where as diffuse damage may not [28, 43, 33]. According to authors in [32], linear microcracks are sheet like defects within the bone matrix that are approximately elliptic in shape.

As stated in [31], accumulation of microdamage can affect the mechanical properties of bone and cause skeletal fragility or stress fractures. Osteocyte apoptosis, due to microdamage or changes in loading, causes surrounding osteocytes to release factors such as RANKL [45, 31, 19]. Furthermore, osteocytes, when they undergo apoptosis, unleash the Wnt canonical pathway.

The purpose of this work is to study the bone remodeling process in cortical bone due to microdamage. This has been done by 1) incorporating the role of osteocytes in the natural initiation of the process, and 2) examining the effects of the Wnt canonical pathway on osteoblastogenesis. Evidence in literature suggests osteocytes have the ability to initiate the bone remodeling process through accumulation of microdamage. The mathematical model found in [8] has been extended to include osteocytes, the Wnt canonical pathway, and its inhibitor sclerostin. Numerical results show the natural initiation of the bone remodeling process through the death of osteocytes from accumulation of microdamge. Additionally, potential therapies for healthy bone remodeling are explored. The paper has been structured into the following sections: model formulation can be found in section 2, followed by theoretical analysis of the model in section 3, section 4 presents numerical results and discussion obtained through MATLAB along with sensitivity analysis for parameters,

and concluding remarks are found in section 5.

2 Model Formulation

Mathematical modeling of complex biological processes is a useful tool that can be used to shed light on the unknown and study hypothesis without physical intervention or cost. There are currently very few mathematical models that have studied the population dynamics of the osteoclasts, osteoblasts, and other cells in their lineage (including osteocytes) in the bone remodeling process.

2.1 Previous Mathematical Modeling

Authors in [22] constructed one of the first temporal models of the population dynamics of osteoclasts and osteoblasts at a single site of bone remodeling. A power law approximation was used to implicitly include the effect of local factors such as the transforming growth factor beta (TGF-β), insulin-like growth factor (IGF), and the RANK-RANKL-OPG pathway. An extension of [22] was also done by authors in [40] which studied the temporal and spatial profiles of RANKL and OPG as they affect the bone remodeling process. This model was able to capture the cutting cone phenomena of a BMU in trabecular bone, and the ability of the RANKL/OPG fields to steer the BMU. Further extensions of [22] were made to study osteocyte-induced targeted bone remodeling [14] . This model studied the population dynamics of active osteoclasts, osteoblasts, and osteocytes. Similar to the Komarova model, it implicitly included the effects of the RANK-RANKL-OPG pathway, the Wnt canonical pathway, and sclerostin through power-law approximation.

The mathematical model constructed in [26] was the first to explicitly include aforementioned factors. This work studied the biochemical control network of the bone remodeling process by using enzyme kinetic reactions (i.e. law of mass action) to

include TGF-β and the RANK-RANKL-OPG pathway. Several metabolic diseases and possible therapies were studied using this model. This model was extended in [37] to include activator/repressor Hill functions to simulate the effects of the factors on the differentiation or apoptosis rates of the cells.

The mathematical model found in [8] was an extension of the [37] model with spatial effects. We explain this model closely in the following subsection.

2.2 Base Spatio-Temporal Model

In this work, we study the targeted bone remodeling process as it occurs within a cortical BMU due to microdamage. We use the framework provided by [8] to study the initiation of the process through the apoptosis of osteocyte cells due to accumulation of microdamage.

The authors developed a 1-D spatial-temporal model to study the organization of cells within the BMU in the presence of biochemical factors such as the RANK-RANKL-OPG pathway, TGF-β, and PTH. Their model was developed using material-balance partial differential equations for active osteoclast (C_a), precursor osteoblast (B_p), active osteoblast (B_a), and TGF-β (T) (see equations 1-5). It was assumed that osteoclasts' travel along the direction of the BMUs progression at a constant speed u and that all other cells and factors have negligible movement in this direction. It was assumed that a capillary forms at the speed at which the osteoclasts progress, u, and that precursor osteoclast, C_p, and uncommited osteoblast, B_u are being provided by the tip of this capillary. A gaussian equation (equation 5) was used to model the local supply of C_p and B_u, where p_{max} is the maximum density of cells at the tip of the capillary, b is the initial position of the capillary tip, and c is the width of the profile of cells. The differentiation rate, D_{C_p}, of osteoclast precursors, C_p, is dependent on RANK-RANKL binding; thus, mass action kinetics was used to determine the

concentration of RANKL (Rl). Furthermore, the apoptosis rate, A_{C_a} of osteoclasts is dependent on the amount of TGF-β in the system. TGF-β was assumed to be released as the osteoclasts resorb bone where α is the concentration of TGF-β found in the bone matrix, k_{res} is the bone volume resorbed per unit time, and D_T is a constant degradation rate. The uncommited osteoblast, B_u, differentiate at a rate $D^T_{B_u}$ which depends on the concentration of TGF-β; similarly, the precursor osteoblast, B_p differentiate into active osteoblast, B_a, at a rate $D^T_{B_p}$ which also depends on TGF-β present in the system. Active osteoblast were assumed to have a constant apoptotic rate A_{B_a}.

$$\frac{\partial C_a}{\partial t} = D_{C_p}\pi^{act}(\frac{Rl}{k^R_{C_p}})C_p - A_{C_a}\pi^{act}(\frac{T}{k^T_{C_a}})C_a - u\frac{\partial C_a}{\partial x} \tag{1}$$

$$\frac{dT}{dt} = \alpha k_{res} C_a - D_T T \tag{2}$$

$$\frac{dB_p}{dt} = D^T_{B_u}\pi^{act}(\frac{T}{k^T_{B_u}})B_u - D^T_{B_p}\pi^{rep}(\frac{T}{k^T_{B_p}})B_p \tag{3}$$

$$\frac{dB_a}{dt} = D^T_{B_p}\pi^{rep}(\frac{T}{k^T_{B_p}})B_p - A_{B_a}B_a \tag{4}$$

$$C_p(x,t) = B_u(x,t) = p_{max}e^{-\frac{(x-ut-b)^2}{2c^2}} \tag{5}$$

Buenzli et al. [8] used hill functions, $\pi^{act}(X)$ and $\pi^{rep}(X)$, are used to represent stimulating (act) or inhibiting (rep) actions that a biochemical factor X has on the differentiation or apoptosis rate of a cell. These functions are expressed as follows, where k is an activation/repression coefficient.

$$\pi^{act}(X) = \frac{X}{1+X} \tag{6}$$

$$\pi^{rep}(X) = \frac{1}{1+X} \tag{7}$$

This model was used to study the organization and structure of cells within the BMU, and is extended in this work to study the initiation of the bone remodeling process in the presence of microdamage.

2.3 Proposed New Spatio-Temporal Model

The mathematical model in [8] gave a fitting framework to study the organization of cells within the BMU in the presence of microdamage. We extend this model to include the primary "sensors" of microdamage found within the bone matrix, namely the osteocytes. Osteocyte apoptosis has been correlated to presence of microdamage in several papers. Additionally, we adjust the model to include other biochemical factors currently believed to play a major role in the process. Sclerostin, secreted by osteocytes, is known to inhibit the Wnt canonical pathway which has recently been found to regulate the commitment and differentiation of cells in the osteoblastic lineage.

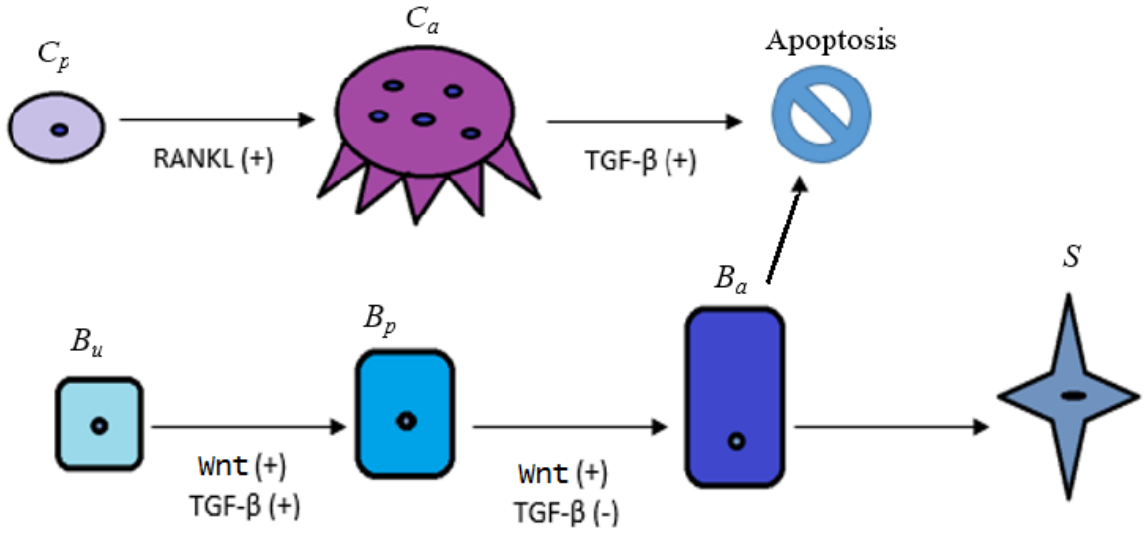

Figure 3. Important factors and their activation (+) or inhibition (-) on the commitment, differentiation, or apoptosis of bone cells.

Our model consists of one partial differential equation and four ordinary differential equations of, arguably, the most important cells and factors in the bone remodeling process. We extend the spatial-temporal model given by [8] by adding an equation for the density of osteocytes in order to study the initiation of targeted bone remodeling process through microdamage. The Wnt canonical pathway, primarily responsible for regulating bone formation, is also integrated in the model. Finally, we adjust the dependence of the ligand and receptor concentration in the RANK-RANKL-OPG pathway on the osteocyte density.

Similar to the previous model, it is assumed that the BMU travels along a longitudinal axis (i.e. along the longitudinal direction of an osteon), x, at a constant speed, u. Within the BMU there is a capillary that grows (also along x) at a speed u and continually supplies osteoclast precursor cells and osteoblast uncommitted progenitors,

where C_p and B_u are the density of cells, through its tip. We assume the local supply of these precursor and progenitor cells is given by the Gaussian equation. Following Buenzli's model, an advection equation is given for the density of active osteoclast cells, C_a, that travel longitudinally (x-direction) along the BMU resorbing old or damaged bone matrix at a constant speed, u.

$$\frac{\partial C_a}{\partial t} = D_{C_p}\pi^{act}(\frac{Rl}{k^R_{C_p}})C_p - A_{C_a}\pi^{act}(\frac{T}{k^T_{C_a}})C_a - u\frac{\partial C_a}{\partial x} \tag{8}$$

$$\frac{dT}{dt} = \alpha k_{res}C_a - D_T T \tag{9}$$

$$\begin{aligned}\frac{dB_p}{dt} =& (D^W_{B_u}\pi^{act}(\frac{W_{B_u}}{k^W_{B_u}}) + D^T_{B_u}\pi^{act}(\frac{T}{k^T_{B_u}}))B_u \\ &- (D^W_{B_p}\pi^{act}(\frac{W_{B_p}}{k^W_{B_p}}) + D^T_{B_p}\pi^{rep}(\frac{T}{k^T_{B_p}}))B_p\end{aligned} \tag{10}$$

$$\begin{aligned}\frac{dB_a}{dt} =& (D^W_{B_p}\pi^{act}(\frac{W_{B_p}}{k^W_{B_p}}) + D^T_{B_p}\pi^{rep}(\frac{T}{k^T_{B_p}}))B_p \\ &- A_{B_a}B_a - D_{B_a}B_a(1 - \frac{S}{S_{max}})\end{aligned} \tag{11}$$

$$\frac{dS}{dt} = D_{B_a}B_a(1 - \frac{S}{S_{max}}) \tag{12}$$

$$C_p(x,t) = B_u(x,t) = p_{max}e^{-\frac{(x-ut-b)^2}{2c^2}} \tag{13}$$

The differentiation rate, D_{C_p}, of the precursor osteoclast cells (C_p) to active osteoclast cells is stimulated by the concentration of RANKL, denoted by Rl, and $k^R_{C_p}$ is the dissociation binding constant. As RANKL binds to RANK (on osteoclast precursor surface), the binding promotes the differentiation of C_p to C_a. OPG inhibits this process by binding to RANKL. It is assumed that the binding rates of these proteins occurs at a much faster rate (than that of the cells) thus the quasi-steady state concentration of RANKL will be determined through the law of mass action in

section 2.4. The apoptosis rate, A_{C_a}, of the active osteoclast cells is stimulated by TGF-β (T) whose equation is given below and dissociation binding constant is $k^T_{C_a}$. Similar to [8] we make the assumption that the rest of the cells or factors have no significant movement along x. It is assumed that TGF-β is released from the bone matrix as the osteoclast cells resorb bone at a rate k_{res}; α is a proportionality constant expressing the TGF-β content stored in the bone. We also assume that TGF-β degrades proportional to its concentration at a rate D_T.

We include ordinary differential equations for the denisities of active osteoblast cells, B_a and their precursors, B_p. The differentiation rate, D_{B_u}, of B_u to B_p is promoted by TGF-β and Wnt binding with co-receptors Frizzled and LRP. Furthermore, differentiation of B_p to B_a is also promoted by the Wnt binding and repressed by the concentration of T; the dissociation binding constants are $k^W_{B_u}$, $k^T_{B_u}$, $k^W_{B_p}$, and $k^T_{B_p}$, respectively. W_{B_u} and W_{B_p} denotes the concentration of Wnt ligands binding to B_u and B_p, respectively; similar to the expression of Rl, we will obtain the quasi-steady state concentration using the law of mass action. We assume that the active osteoblasts are removed from the system through apoptosis or by becoming embedded in the bone matrix and differentiation into osteocytes; A_{B_a} is the constant rate of apoptosis for the osteoblasts. We assume that some of osteoblasts will become embedded in the bone matrix and differentiate into osteocytes at a rate D_{B_a} and a limiting term is added to account for the limited space available in cortical bone for new osteocytes to form. We denote the maximum density of osteocytes as S_{max}. We also use hill functions, $\pi^{act}(X)$ and $\pi^{rep}(X)$, to represent stimulating (act) or inhibiting (rep) actions that a biochemical factor X has on the commitment, differentiation, or apoptosis rate of a cell. Thus, excluding the expressions for RANKL and Wnt which are developed in section 2.4, our model consists of equations 8-13.

2.4 Signaling Pathways

As mentioned previously, hill functions are used to include the effects of biochemical factors on the differentiation and apoptosis of cells; we can see the activation (+) or inhibition (−) of the factors and state variables in Figure 3. These biochemical factors come in the form of ligands in signaling pathways or growth factors such as TGF-β. Due to the fast reaction rates of the ligands binding to their receptors on cells for the RANK-RANKL-OPG and Wnt canonical pathways, we use the principle of mass action kinetics to determine the quasi-steady state concentration of the ligand for each respective pathway as is presented in [25].

2.4.1 Mass Action Kinetics - RANKL Concentration

The RANK-RANKL-OPG pathway can be seen as the following reversible reactions in equations 14 and 15, where RANK, RANKL, and OPG are denoted by R, Rl, and O, respectively; A_{RRl}, A_{ORl} are complexes.

$$R + Rl \rightleftharpoons A_{RRl} \tag{14}$$

$$O + Rl \rightleftharpoons A_{ORl} \tag{15}$$

We assume that there are a constant number of RANK receptors on the surface of osteoclast precursor, N_R. We can develop ODEs for the rate of reactions using mass action kinetics (equations 17-20). Production and degradation terms are included for RANKL and OPG: P_Rl, P_O, D_{Rl}, D_O.

$$R = N_R C_p \tag{16}$$

$$\frac{dO}{dt} = -k_1 RlO + k_2 A_{ORl} + P_O + D_O \tag{17}$$

$$\frac{dRl}{dt} = -k_1 RlO + k_2 A_{ORl} - k_3 RlR + k_4 A_{RRl} + P_{Rl} + D_{Rl} \tag{18}$$

$$\frac{dA_{ORl}}{dt} = k_1 RlO - k_2 A_{ORl} \tag{19}$$

$$\frac{dA_{RRl}}{dt} = k_3 RlR - k_4 A_{RRl} \tag{20}$$

Since it is assumed that the binding reactions occur much more quickly than the change in cell concentration we obtain equations 21 and 22.

$$P_O + D_O = 0 \tag{21}$$

$$P_{Rl} + D_{Rl} = 0 \tag{22}$$

Parathyroid hormone, PTH, is a well-known regulator of the RANK-RANKL-OPG pathway [37] and is assumed to be provided homogeneously along the BMU. Repression of OPG and activation of RANKL by PTH is given by π^{rep}_{PTH,B_a} and π^{act}_{PTH,B_p}, respectively. The production and degradation of OPG are expressed in equations 23 and 24 where β_O is the OPG production rate of active osteoblasts, O_{max} is the maximum possible amount of OPG, and $\hat{D}_O$ is the rate of degradation of OPG. The concentration of OPG is found in equation 25.

$$P_O = \beta_O B_a \pi^{rep}_{PTH,B_a}(1 - \frac{O}{O_{max}}) \tag{23}$$

$$D_O = -\hat{D}_O O \tag{24}$$

$$O = \frac{\beta_O B_a \pi^{rep}_{PTH,B_a} O_{max}}{\hat{D}_O O_{max} + \beta_O B_a \pi^{rep}_{PTH,B_a}} \tag{25}$$

Similarly, the production and degradation of RANKL are expressed in equations 26 and 27 where β_{Rl} is the RANKL production rate of osteoblast precursors, $Rl_{present}$

is the total concentration of RANKL in free or complex form, Rl_{max} is the maximum concentration of RANKL that is found on the surface of the osteoblast precursors and released by apoptotic osteocytes, and $\hat{D}_{Rl}$ is the rate of degradation of RANKL.

$$P_{Rl} = \beta_{Rl}(1 - \frac{Rl_{present}}{Rl_{max}}) \tag{26}$$

$$D_{Rl} = -\hat{D}_{Rl} Rl_{present} \tag{27}$$

$$Rl_{present} = Rl + [Rl - O] + [Rl - R] = Rl(1 + K_{A_1} O + K_{A_2} R) \tag{28}$$

$$Rl_{max} = R_1 B_p \pi^{act}_{PTH,B_p} + R_2(S_{max} - S)\pi^{act}_{PTH,S} \tag{29}$$

$$Rl = \frac{\beta_{Rl}(R_1 B_p \pi^{act}_{PTH,B_p} + R_2(S_{max} - S))}{(1 + K_{A_1} O + K_{A_2} R)(\beta_{Rl} + \hat{D}_{Rl}(R_1 B_p \pi^{act}_{PTH,B_p} + R_2(S_{max} - S)\pi^{act}_{PTH,S}))} \tag{30}$$

2.4.2 Mass Action Kinetics - Wnt Concentration

A similar approach can be taken when deriving the expression for the Wnt ligand, W. One main difference from the RANK-RANKL-OPG pathway is that the Wnt canonical pathway has two co-receptors, LRP (L) and Frizzled (F). The Wnt ligand binds to Frizzled, then binds to LRP to form a trenary complex that inhibits degradation of β-catenin (see section 1.2). Sclerostin (Scl) is expressed by osteocytes and inhibits the pathway by binding to the LRP co-receptor. Equations 31-33 show the reversible reactions for the Wnt canonical pathway.

$$W + F \rightleftharpoons A_{WF} \tag{31}$$

$$A_{WF} + L \rightleftharpoons A_{WFL} \tag{32}$$

$$Scl + L \rightleftharpoons A_{SclL} \tag{33}$$

We assume that there are a constant number of Frizzled and LRP receptors on the surface of uncommited progenitors ,B_u, and precursors of the osteoblastic lineage, B_p (N_F and N_L, respectively). ODEs for the rate of reactions using mass action kinetics as shown in equations 34-37. Production and degradation terms are included for Wnt and Sclerostin: P_W, P_{Scl}, D_W, D_{Scl}.

$$\frac{dW}{dt} = -k_5 WF + k_6 A_{WF} + P_W + D_W \tag{34}$$

$$\frac{dA_{WF}}{dt} = -k_6 A_{WF} + k_5 WF - k_7 A_{WF} L + k_8 A_{WFL} \tag{35}$$

$$\frac{dScl}{dt} = -k_9 SclL + k_{10} A_{SclL} + P_{Scl} + D_{Scl} \tag{36}$$

$$\frac{dA_{SclL}}{dt} = k_9 SclL - k_{10} A_{SclL} \tag{37}$$

Once again, finding the quasi-steady state of W and Scl we obtain equations 38 and 39.

$$P_W + D_W = 0 \tag{38}$$

$$P_{Scl} + D_{Scl} = 0 \tag{39}$$

The production and degradation of sclerostin are expressed in equations 40 and 41 where β_{Scl} is the sclerostin production rate of osteocytes, Scl_{max} is the maximum possible amount of sclerostin, and $\hat{D}_{Scl}$ is the rate of degradation of sclerostin. The concentration of sclerostin is found in equation 42.

$$P_{Scl} = \beta_{Scl} S(1 - \frac{Scl}{Scl_{max}}) \tag{40}$$

$$D_{Scl} = -\hat{D}_{Scl} Scl \tag{41}$$

$$Scl = \frac{\beta_{Scl} S Scl_{max}}{\hat{D}_{Scl} Scl_{max} + \beta_{Scl} S} \tag{42}$$

Wnt ligands are expressed by osteocytes, however, without the presence of apoptotic ostocytes (microdamage) the Wnt canonical pathway cannot be unleashed. Equation 43 gives the production of Wnt, where β_W is the Wnt production rate of osteocytes, $W_{present}$ is the total concentration of Wnt in free or bound form, and W_{max} is the maximum concentration of Wnt expressed by osteocytes.

$$P_W = \beta_W (1 - \frac{S}{S_{max}})(1 - \frac{W_{present}}{W_{max}}) \tag{43}$$

$$W_{present} = W + K_{B_1} WF + W K_{B_2} FL \tag{44}$$

$$W_{max} = R_3 S \tag{45}$$

$$D_W = -\hat{D}_W W_{present} \tag{46}$$

Equation 47 gives the expression of the concentration of Wnt ligands. The equation is modified in order to incorporate the concentration of sclerostin by finding the total amount of LRP in the system and solving for the LRP concentration. However, taking into account that we have Frizzled and LRP receptors on both B_u and B_p, we separate the expression of W into W_{B_u} and W_{B_p} which represents the Wnt ligands available to bind with receptors on the surface of B_u and B_p, respectively (see equations 52 and 53).

$$W = \frac{\beta_W(1 - \frac{S}{S_{max}})R_3S}{(1 + K_{B_1}F + K_{B_2}FL)(\beta_W(1 - \frac{S}{S_{max}}) + \hat{D}_W R_3 S)} \tag{47}$$

$$F_{B_u} = N_F B_u \tag{48}$$

$$F_{B_p} = N_F B_p \tag{49}$$

$$L_{B_u} = \frac{N_L B_u}{1 + K_{B_2}F_{B_u} + K_{B_3}Scl} \tag{50}$$

$$L_{B_p} = \frac{N_L B_p}{1 + K_{B_2}F_{B_p} + K_{B_3}Scl} \tag{51}$$

$$W_{B_u} = \frac{\beta_W(1 - \frac{S}{S_{max}})R_3S}{(1 + K_{B_1}F_{B_u} + K_{B_2}F_{B_u}L_{B_u})(\beta_W(1 - \frac{S}{S_{max}}) + \hat{D}_W R_3 S)} \tag{52}$$

$$W_{B_p} = \frac{\beta_W(1 - \frac{S}{S_{max}})R_3S}{(1 + K_{B_1}F_{B_p} + K_{B_2}F_{B_p}L_{B_p})(\beta_W(1 - \frac{S}{S_{max}}) + \hat{D}_W R_3 S)} \tag{53}$$

Our proposed system consists of spatio-temporal equations that includes some of the most important signaling pathways currently known. This model allows us to study the initiation of the BMU through apoptotic osteocytes due to microdamage, and the effects of the signaling pathways. The following tables provide descriptions for the parameters within the main PDE model, the RANK-RANKL-OPG pathway, and the Wnt canonical pathway.

Table 1. Parameter definitions for main PDE model

Symbol	Description
D_{C_p}	maximum differentiation rate of C_p
$k_{C_p}^R$	dissociation binding constant for RANKL binding on C_p
$D_{B_u}^T$	maximum differentiation rate of B_u due to TGF-β
$D_{B_u}^W$	maximum differentiation rate of B_u due to Wnt pathway
$k_{B_u}^T$	dissociation binding constant for $TGF-\beta$ binding on B_u
$k_{B_u}^W$	dissociation binding constant for Wnt binding on B_u
A_{C_a}	maximum apoptosis rate of C_a
$k_{C_a}^T$	dissociation binding constant for $TGF-beta$ binding on C_a
$D_{B_p}^W$	maximum differentiation rate of B_p due to Wnt Pathway
$k_{B_p}^W$	dissociation binding constant for Wnt binding on B_p
$D_{B_p}^T$	maximum differentiation rate of B_p due to $TGF-\beta$
$k_{B_p}^T$	dissociation binding constant for $TGF-\beta$ binding on B_p
A_{B_a}	apoptosis rate of B_a
α	concentration of $TGF-\beta$ found in the bone matrix
k_{res}	bone volume resorbed per unit time by a single osteoclast
D_T	degradation rate of $TGF-\beta$
D_{B_a}	rate at which B_a becomes embedded in bone
u	average speed of the BMU's progression
p_{max}	maximum concentration of B_u or C_p at the tip of the capilary
b	initial position of the tip of the capillary
c	width of the gaussian curve

Table 2. Parameter definitions for RANK-RANKL-OPG Pathway

Symbol	Description
β_{Rl}	production rate of RANKL
$\hat{D}_{Rl}$	degradation rate of RANKL
R_1	maximum number of RANKL on the surface of B_p
R_2	maximum concentration of RANKL produced per S
π^{act}_{PTH,B_p}	activation parameter for RANKL related to PTH on B_p
$\pi^{act}_{PTH,S}$	activation parameter for RANKL related to PTH on S
K_{A_1}	association binding constant for RANKL-OPG
O_{max}	maximum possible OPG concentration
β_O	production rate of OPG
π^{rep}_{PTH,B_a}	repressions parameter for OPG related to PTH on B_a
$\hat{D}_O$	degradation rate of OPG
K_{A_2}	association binding constant for RANK-RANKL
N_R	number of RANK receptors expressed on C_p

Table 3. Parameter definitions for Wnt Canonical Pathway

Symbol	Description
β_W	production rate of Wnt
R_3	maximum concentration of Wnt produced per S
K_{B_1}	association binding constant for Wnt-Frizzled
N_F	number of Frizzled receptors expressed on B_u and B_p
K_{B_2}	association binding constant for Wnt-Frizzled-LRP
N_L	number of LRP receptors expressed on B_u and B_p
K_{B_3}	association binding constant for LRP-sclerostin
β_{Sc}	production rate of sclerostin
Sc_{max}	maximum possible sclerostin concentration
$\hat{D}_{Sc}$	degradation rate of sclerostin
$\hat{D}_W$	degradation rate of Wnt

3 Model Analysis and Comparison

Our model consists of one partial differential equation (PDE) and four ordinary differential equations (ODEs), as seen in equations 8-13. In order to perform equilibria and stability analysis of the system, we transform our equations into a purely autonomous ODE system by removing the advection term in the active osteoclast equation, C_a. Furthermore, since the precursor gaussian equation depends on space and time, we make a simplifying assumption that the cells, C_p and B_u, can be expressed as an exponentially decaying function as the tip of the capillary passes through a particular point, $\hat{x} = b$. We lump together C_p and B_u into a single variable P. Thus P can be written as an ODE as in equation 54, where f will depend on the differentiation rate of the cells into active osteoclasts and osteoblasts along with a adjusting constant that will account for the profile of the local supply of cells given by the gaussian equation as it passes through a point, $\hat{x} = b$.

$$\frac{dP}{dt} = -fP \tag{54}$$

3.1 Simplified ODE System 1

In this section we simplify our system to a system of three ODEs (P, C_a, B_a). We assume that all other state variables (B_p, T, and S) are constant; the hill functions, expressing the signaling pathways, are also considered constants. Different variables are used for the differentiation and apoptosis rates for simplification.

$$\frac{dP}{dt} = f_1(-a_1P - a_2P) \tag{55}$$

$$\frac{dC_a}{dt} = a_1P - a_3C_a \tag{56}$$

$$\frac{dB_a}{dt} = a_2P - a_4B_a - a_5B_a \tag{57}$$

To analyze the system, we find the single equilibrium $E_1 = (P^*, {C_a}^*, {B_a}^*) = (0,0,0)$, and the Jacobian, $J(E_1)$. Since this is a lower-triangular matrix, the diagonal entries are the eigenvalues for the Jacobian. We note that the eigenvalues are all negative, thus E_1 is a stable equilibrium.

$$J(E_1) = \begin{bmatrix} -f_1(a_1 + a_2) & 0 & 0 \\ a_1 & -a_3 & 0 \\ a_2 & 0 & -a_4 - a_5 \end{bmatrix}$$

It is expected that once the precursor cells, P, have left the remodeling site, $\hat{x}$, the active osteoclasts and osteoblasts will remove old bone and form new bone, respectively, then leave the site. The solution for this system (equations 58-60) verifies the stable equilibrium and stability of the system.

$$P(t) = P(0)e^{-f_1(a_1+a_2)t} \tag{58}$$

$$C_a(t) = C_a(0)e^{-a_3t} - P(0)\frac{a_1}{a_1 + a_2 - a_3}e^{-a_3t}(e^{(a_3-a_1-a_2)t} - 1) \tag{59}$$

$$B_a(t) = B_a(0)e^{-a_4t} - P(0)\frac{a_2}{a_1 + a_2 - a_4}e^{-a_4t}(e^{(a_4-a_1-a_2)t} - 1) \tag{60}$$

3.2 Simplified ODE System 1a

The previous system 1 is modified by no longer assuming that the RANK-RANKL-OPG signaling pathway is constant, as follows.

$$\frac{dP}{dt} = f_{1a}(-a_1 \frac{Rl}{k_1 + Rl} P - a_2 P) \tag{61}$$

$$\frac{dC_a}{dt} = a_1 \frac{Rl}{k_1 + Rl} P - a_3 C_a \tag{62}$$

$$\frac{dB_a}{dt} = a_2 P - a_4 B_a - a_5 B_a \tag{63}$$

$$Rl = \frac{b_1 P + b_2}{(1 + \frac{b_3 B_a}{b_4 + b_5 B_a} + b_6 P)(b_7 + b_8 P)} \tag{64}$$

A single biologically meaningful equilibrium is found: $E_2 = (P^*,\ {C_a}^*,\ {B_a}^*)$ = (0,0,0). Similar to the previous model, the Jacobian, $J(E_2)$, indicates a stable equilibrium.

$$J(E_2) = \begin{bmatrix} f_{1a}(-\frac{a_1 b_2}{k_1 b_7 + b_2} - a_2) & 0 & 0 \\ \frac{a_1 b_2}{k_1 b_7 + b_2} & -a_3 & 0 \\ a_2 & 0 & -a_4 - a_5 \end{bmatrix}$$

3.3 Simplified ODE System 1b

ODE system 1b, we remove the assumption that the Wnt Canonical Pathway is constant.

$$\frac{dP}{dt} = f_{1b}(-a_1\frac{Rl}{k_1+Rl}P - a_2\frac{W}{k_2+W}P) \tag{65}$$

$$\frac{dC_a}{dt} = a_1\frac{Rl}{k_1+Rl}P - a_3C_a \tag{66}$$

$$\frac{dB_a}{dt} = a_2\frac{W}{k_2+W}P - a_4B_a - a_5B_a \tag{67}$$

$$Rl = \frac{b_1P + b_2}{(1+\frac{b_3B_a}{b_4+b_5B_a} + b_6P)(b_7+b_8P)} \tag{68}$$

$$W = \frac{c_7}{c_{10}(1+c_8P+c_9P(\frac{c_1P}{c_3+c_5P}))} \tag{69}$$

A single biologically meaningful equilibrium is found: $E_3 = (P^*,\ {C_a}^*,\ {B_a}^*) = (0,0,0)$. Similar to the previous model, the Jacobian, $J(E_3)$, indicates a stable equilibrium.

$$J(E_3) = \begin{bmatrix} f_{1b}(-\frac{a_1b_2}{k_1b_7+b_2} - \frac{a_2c_1}{k_2(c_2+c_7)+c_1}) & 0 & 0 \\ \frac{a_1b_2}{k_1b_7+b_2} & -a_3 & 0 \\ \frac{a_2c_1}{k_2(c_2+c_7)+c_1} & 0 & -a_4-a_5 \end{bmatrix}$$

3.4 Simplified ODE System 2

Subsections 3.4-3.6 incorporate an ODE for the osteocyte density. We begin by considering both signaling pathways as constants for this system.

$$\frac{dP}{dt} = f_2(-a_1P - a_2P) \tag{70}$$

$$\frac{dC_a}{dt} = a_1P - a_3C_a \tag{71}$$

$$\frac{dB_a}{dt} = a_2P - a_4B_a - a_5B_a(1-\frac{S}{a_6}) \tag{72}$$

$$\frac{dS}{dt} = a_5B_a(1-\frac{S}{a_6}) \tag{73}$$

After analysis, we determing that ODE system 2 has a line of non-isolated equilibria along the $S-$dimension: $E_4 = (P^*,\ {C_a}^*,\ {B_a}^*,\ S^*) = (0,0,0,\ S^{free})$. The Jacobian for this system is as follows.

$$J(E_4) = \begin{bmatrix} f_2(-a_1 - a_2) & 0 & 0 & 0 \\ a_1 & -a_3 & 0 & 0 \\ a_2 & 0 & -a_4 - a_5(1 - \frac{S^{free}}{a_6}) & 0 \\ 0 & 0 & a_5(1 - \frac{S^{free}}{a_6}) & 0 \end{bmatrix}$$

We note that the Jacobian matrix is lower-triangular; the diagonal entries of the matrix are the eigenvalues $\lambda = f_2(-a_1 - a_2), -a_3, -a_4 - a_5(1 - \frac{S^{free}}{a_6}), 0$. $J(E_4)$ has three negative eigenvalues and one zero eigenvalue, thus we classify the line of non-isolated equilibria as an attracting line.

3.5 Simplified ODE System 2a

ODE system 2a removes the assumption that the RANK-RANKL-OPG pathway is constant.

$$\frac{dP}{dt} = f_{2a}(-a_1 \frac{Rl}{k_1 + Rl} P - a_2 P) \tag{74}$$

$$\frac{dC_a}{dt} = a_1 \frac{Rl}{k_1 + Rl} P - a_3 C_a \tag{75}$$

$$\frac{dB_a}{dt} = a_2 P - a_4 B_a - a_5 B_a (1 - \frac{S}{a_6}) \tag{76}$$

$$\frac{dS}{dt} = a_5 B_a (1 - \frac{S}{a_6}) \tag{77}$$

$$Rl = \frac{b_1 P + b_2(a_6 - S)}{(1 + \frac{b_3 B_a}{b_4 + b_5 B_a} + b_6 P)(b_7 + b_8 P + b_9(a_6 - S))} \tag{78}$$

Similar to the previous ODE system, ODE system 2a has a line of non-isolated equilibria along the $S-$dimension: $E_5 = (P^*, C_a{}^*, B_a{}^*, S^*) = (0,0,0, S^{free})$.

$$J(E_5) = \begin{bmatrix} \gamma_1 & 0 & 0 & 0 \\ \gamma_2 & -a_3 & 0 & 0 \\ a_2 & 0 & -a_4 - a_5(1 - \frac{S^{free}}{a_6}) & 0 \\ 0 & 0 & a_5(1 - \frac{S^{free}}{a_6}) & 0 \end{bmatrix}$$

$$\gamma_1 = f_{2a}(-a_1(\frac{b_2(a_6 - S^{free})}{k_1(b_7 + b_9(a_6 - S^{free})) + b_2(a_6 - S^{free})}) - a_2)$$

$$\gamma_2 = a_1(\frac{b_2(a_6 - S^{free})}{k_1(b_7 + b_9(a_6 - S^{free})) + b_2(a_6 - S^{free})})$$

We note that the Jacobian matrix, $J(E_5)$, is lower-triangular; the diagonal entries of the matrix are the eigenvalues $\lambda = \gamma_1, -a_3, -a_4 - a_5(1 - \frac{S^{free}}{a_6}), 0$. Equilibrium E_5 is classified as an attracting line of non-isolated equilibria.

3.6 Simplified ODE System 2b

ODE system 2b includes both the RANK-RANKL-OPG and Wnt canonical pathways as shown in equations 79-84.

$$\frac{dP}{dt} = f_{2b}(-a_1\frac{Rl}{k_1+Rl}P - a_2\frac{W}{k_2+W}P) \tag{79}$$

$$\frac{dC_a}{dt} = a_1\frac{Rl}{k_1+Rl}P - a_3C_a \tag{80}$$

$$\frac{dB_a}{dt} = a_2\frac{W}{k_2+W}P - a_4B_a - a_5B_a(1-\frac{S}{a_6}) \tag{81}$$

$$\frac{dS}{dt} = a_5B_a(1-\frac{S}{a_6}) \tag{82}$$

$$Rl = \frac{b_1P + b_2(a_6-S)}{(1+\frac{b_3B_a}{b_4+b_5B_a}+b_6P)(b_7+b_8P+b_9(a_6-S))} \tag{83}$$

$$W = \frac{c_1S(1-\frac{S}{a_6})}{c_2S(1+c_3P+c_4P(c_5P-c_6\frac{S}{c_7S+c_8}))+c_9(1-\frac{S}{a_6})} \tag{84}$$

Similar to previous systems, ODE system 2b has a line of non-isolated equilibria along the $S-$dimension: $E_6 = (P^*, {C_a}^*, {B_a}^*, S^*) = (0,0,0, S^{free})$.

$$J(E_6) = \begin{bmatrix} \gamma_3 & 0 & 0 & 0 \\ \gamma_4 & -a_3 & 0 & 0 \\ \gamma_5 & 0 & -a_4 - a_5(1-\frac{S^{free}}{a_6}) & 0 \\ 0 & 0 & a_5(1-\frac{S^{free}}{a_6}) & 0 \end{bmatrix}$$

$$\begin{aligned}
\gamma_3 =& f_{2b}(-a_1(\frac{b_2(a_6-S^{free})}{k_1(b_7+b_9(a_6-S^{free}))+b_2(a_6-S^{free})}) \\
&- a_2(\frac{c_7(a_6-S^{free})S^{free}}{k_2(c_10(a_6-S^{free})+c_{11}a_6S^{free})+c_7(a_6-S^{free})S^{free}}))\\
\gamma_4 =& a_1(\frac{b_2(a_6-S^{free})}{k_1(b_7+b_9(a_6-S^{free}))+b_2(a_6-S^{free})})\\
\gamma_5 =& a_2(\frac{c_7(a_6-S^{free})S^{free}}{k_2(c_10(a_6-S^{free})+c_{11}a_6S^{free})+c_7(a_6-S^{free})S^{free}})
\end{aligned}$$

We note that the Jacobian matrix is lower-triangular; the diagonal entries of the matrix are the eigenvalues $\lambda = \gamma_3, -a_3, -a_4 - a_5(1 - \frac{S^{free}}{a_6}), 0$. $J(E_6)$ is found to have three negative eigenvalues and one zero eigenvalue, thus it has an attracting line of non-isolated equilibria.

3.7 Complete ODE System

Our final simplification of the PDE system includes both signaling pathways and all state variables found in our model (equations 8-13). The main difference between our model and this ODE system, is that an ODE is used to model the precursor cells rather than the gaussian expression.

$$\frac{dP}{dt} = f_F(-a_1\frac{Rl}{k_1 + Rl}P - (a_2\frac{W_P}{k_2 + W_P} + a_7\frac{T}{k_3 + T})P) \tag{85}$$

$$\frac{dC_a}{dt} = a_1\frac{Rl}{k_1 + Rl}P - a_3\frac{T}{k_4 + T}C_a \tag{86}$$

$$\frac{dB_p}{dt} = (a_2\frac{W_P}{k_2 + W_P} + a_7\frac{T}{k_3 + T})P - (a_{11}\frac{W_{B_p}}{k_6 + W_{B_p}} + a_8\frac{k_5}{k_5 + T})B_p \tag{87}$$

$$\frac{dB_a}{dt} = (a_{11}\frac{W_{B_p}}{k_6 + W_{B_p}} + a_8\frac{k_5}{k_5 + T})B_p - a_4B_a - a_5B_a(1 - \frac{S}{a_6}) \tag{88}$$

$$\frac{dT}{dt} = a_9C_a - a_{10}T \tag{89}$$

$$\frac{dS}{dt} = a_5B_a(1 - \frac{S}{a_6}) \tag{90}$$

$$Rl = \frac{b_1B_p + b_2(a_6 - S)}{(1 + \frac{b_3B_a}{b_4 + b_5B_a} + b_6P)(b_7 + b_8B_p + b_9(a_6 - S))} \tag{91}$$

$$W_P = \frac{c_1S(1 - \frac{S}{a_6})}{c_2S(1 + c_3P + c_4P(c_5P - c_6\frac{S}{c_7S + c_8})) + c_9(1 - \frac{S}{a_6})} \tag{92}$$

$$W_{B_p} = \frac{c_1S(1 - \frac{S}{a_6})}{c_2S(1 + c_3B_p + c_4B_p(c_5B_p - c_6\frac{S}{c_7S + c_8})) + c_9(1 - \frac{S}{a_6})} \tag{93}$$

It is determined that this system has a line of non-isolated equilibria along the $S-$dimension: $E_7 = (P^*, {C_a}^*, {B_p}^*, {B_a}^*, T^*, S^*) = (0,0,0,0,0, S^{free})$. We compute the Jacobian matrix and obtain $J(E_7)$.

$$J(E_7) = \begin{bmatrix} \gamma_6 + \gamma_7 & 0 & 0 & 0 & 0 & 0 \\ \gamma_8 & 0 & 0 & 0 & 0 & 0 \\ \gamma_9 & 0 & \gamma_{10} & 0 & 0 & 0 \\ 0 & 0 & -\gamma_{10} & -a_4 - a_5(1 - \frac{S^{free}}{a_6}) & 0 & 0 \\ 0 & a_9 & 0 & 0 & -a_{10} & 0 \\ 0 & 0 & 0 & a_5 & 0 & 0 \end{bmatrix}$$

$$\gamma_6 = f_F(-a_1(\frac{b_2(a_6 - S^{free})}{k_1(b_7 + b_9(a_6 - S^{free})) + b_2(a_6 - S^{free})}))$$

$$\gamma_7 = f_F(-a_2(\frac{c_1 S^{free}(1 - S^{free}/a_6)}{k_2(c_2 S^{free} + c_9(1 - S^{free}/a_6)) + c_1 S^{free}(1 - S^{free}/a_6)}))$$

$$\gamma_8 = a_1(\frac{b_2(a_6 - S^{free})}{k_1(b_7 + b_9(a_6 - S^{free})) + b_2(a_6 - S^{free})})$$

$$\gamma_9 = a_2(\frac{c_1 S^{free}(1 - S^{free}/a_6)}{k_2(c_2 S^{free} + c_9(1 - S^{free}/a_6)) + c_1 S^{free}(1 - S^{free}/a_6)})$$

$$\gamma_{10} = -a_{11}(\frac{c_1 S^{free}(1 - S^{free}/a_6)}{k_6(c_2 S^{free} + c_9(1 - S^{free}/a_6)) + c_1 S^{free}(1 - S^{free}/a_6)}) - a_8$$

This Jacobian matrix is lower-triangular with diagonal entries (and eigenvalues): $\lambda = \gamma_6, 0, 0, -a_4 - a_5(1 - \frac{S^{free}}{a_6}), -a_{10}, 0$. Similar to the simplified ODE systems, it is determined that the line of non-isolated equilibria is an attracting line.

3.8 Comparison of ODE and PDE Models

As mentioned previously, simplifications were made in order to transform our PDE model to an autonomous ODE model. One of those simplifications consisted of no longer modeling our precursor cells through a gaussian equation, but rather presenting it as an exponentially decaying equation 54 that decayed at a rate f, where f depends on the differentiation of P to B_a and C_a and an adjusting constant to fit the shape of the gaussian equation. The adjusting constants varied for each of the models.

Figure 4 shows the comparison between models 1, 1a, and 1b. Although the end behavior of models is the same, we see that system 1 has a very large concentration of osteoclast and osteoblast. This is expected, since introducing the RANK-RANKL-OPG pathway reduces the differentiation rate of P. Similarly, introducing the Wnt canonical pathway reduces the differentiation rate of P. This also occurs for systems 2, 2a, and 2b as is seen in Figure 5. Osteocyte cell concentration reaches the maximum concentration quickly for systems 2 and 2a, but because of the lower differentiation rates in system 2b, S approaches the maximum concentration much slower. The lifespan of a BMU is approximately 6 - 9 months, making the simplified systems unrealistic [27].

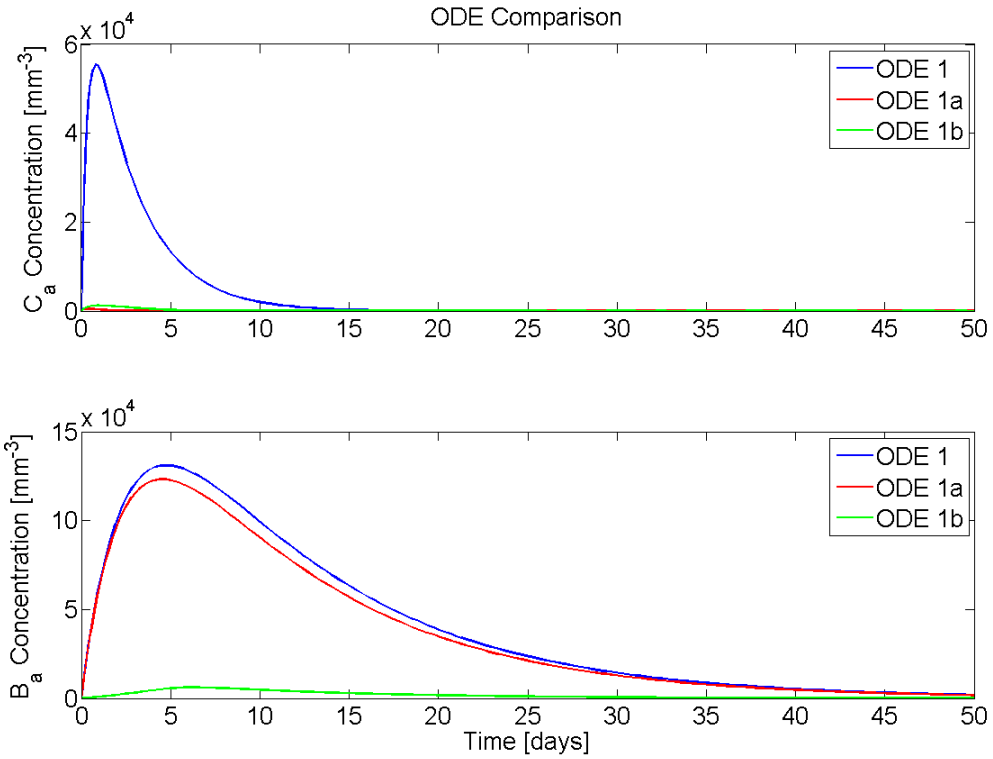

Figure 4. Model Comparison of Simplified ODE Systems 1, 1a, and 1b.

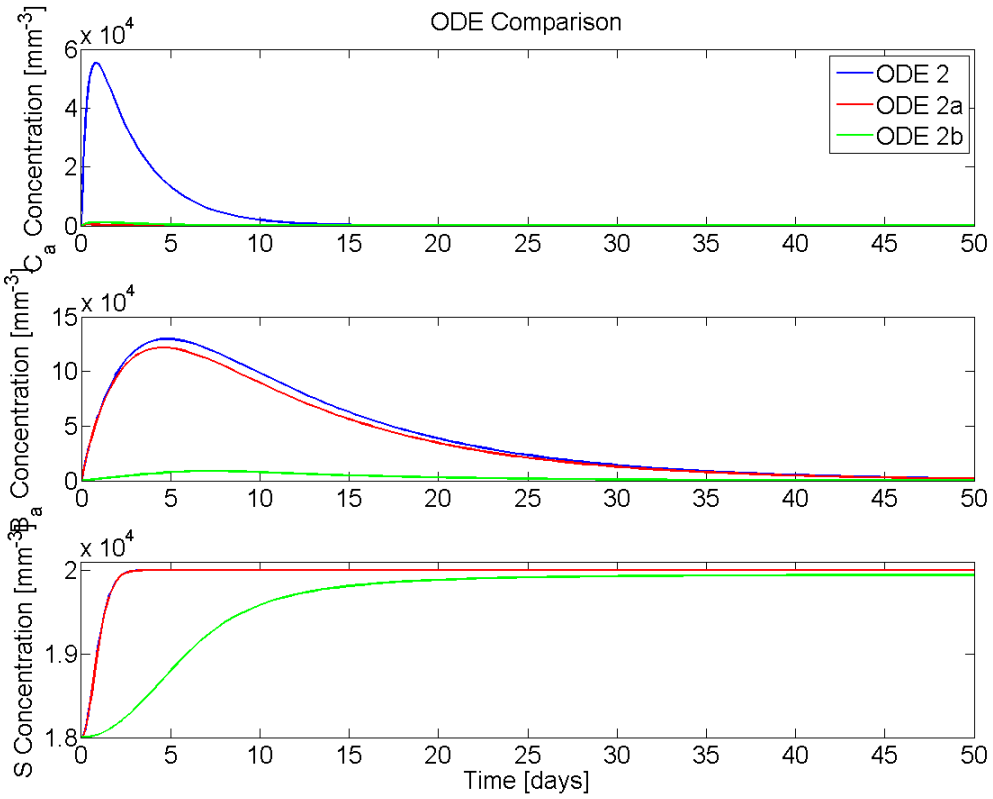

Figure 5. Model Comparison of Simplified ODE Systems 2, 2a, and 2b.

Figure 6 shows that the complete ODE system is a very good representation of the PDE model (with spatial homogeneity). There are small differences in maximum concentrations of osteoclast and osteoblast cells that can be attributed to the adjusting factor, f_F. With this analysis we can conclude that the PDE system will reach any equilibrium (C_a^*, B_p^*, B_a^*,T^*, S^*) = (0,0,0,0,0, S^{free}). The set of parameters chosen for the results in this section allowed us to reach the maximum density of osteocytes; the following section presents further study of our PDE model with this and other sets of parameters (parameter values for this section found in Appendix A). Although the ODE system closely models the spatially-homogeneous PDE model, the

PDE model gives the advantage of being able to consider non-spatially homogeneous intial conditions; i.e. we can consider spatially-dependent initial microcracks.

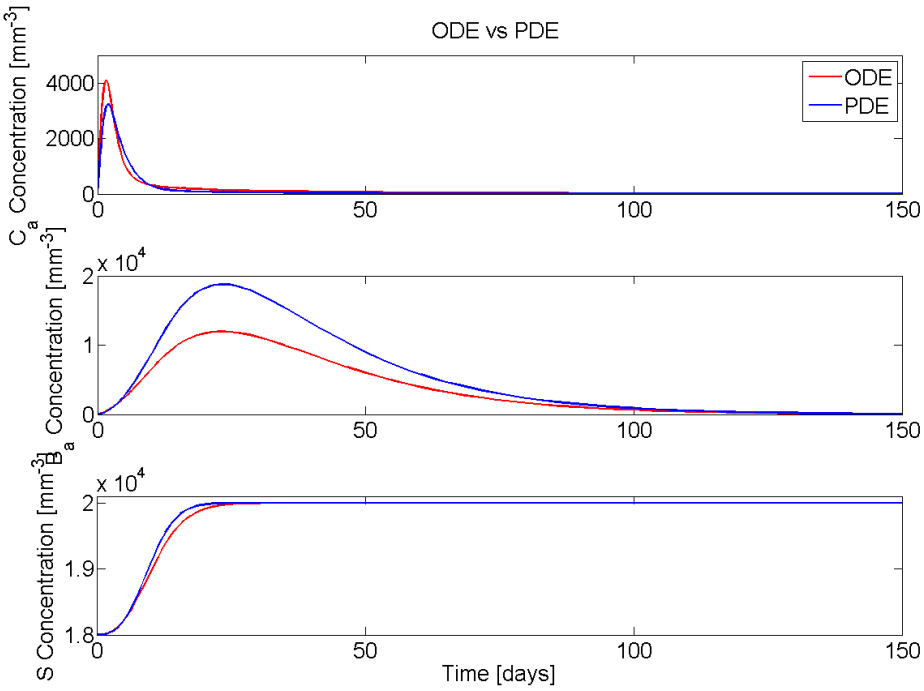

Figure 6. Model Comparison of the Complete ODE System with the PDE system.

3.9 Sensitivity Analysis

Local sensitivity analysis was performed to determine how variations in each parameter impact changes in four model outputs: 1) the time to remodel, T_{final}, 2) the final osteocyte density, S_{final}, 3) the maximum osteoblast and 4) the maximum osteoclast density, Ba_{max} and Ca_{max}. Since no analytic expression exists for any of the model outputs, we estimate the sensitivity index numerically (see Equation 94 where SI represents the sensitivity index). This sensitivity index is described further in [1]. This local method calculates SI for a single parameter while fixing all other parameters. In comparison to global methods which consider big and small

changes in all parameters, local methods consider only small changes in individual parameters. This has limitations, but is considered more efficient for small systems with no discontinuities [41]. Thus, we discuss the sensitivity index for a ±1% change in individual parameter values (see Figures 7-12). Varying changes in parameters were considered and can be found in Appendix B.

$$SI = \frac{\delta u}{\delta p}\frac{p}{u} \approx \frac{\Delta u}{\Delta p}\frac{p}{u} \tag{94}$$

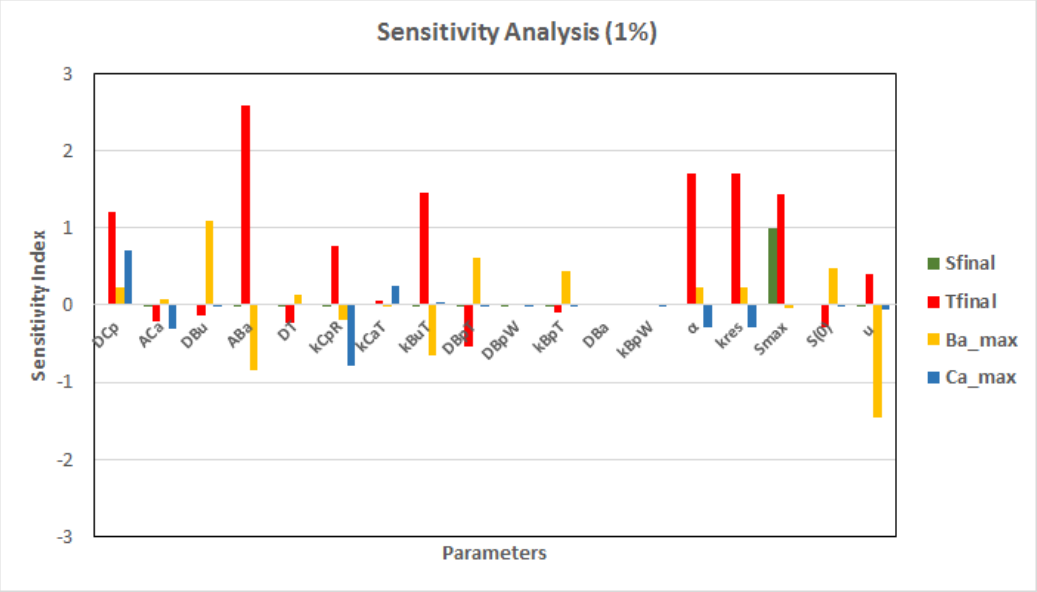

Figure 7. Sensitivity analysis for a 1% increase in parameters in the main model.

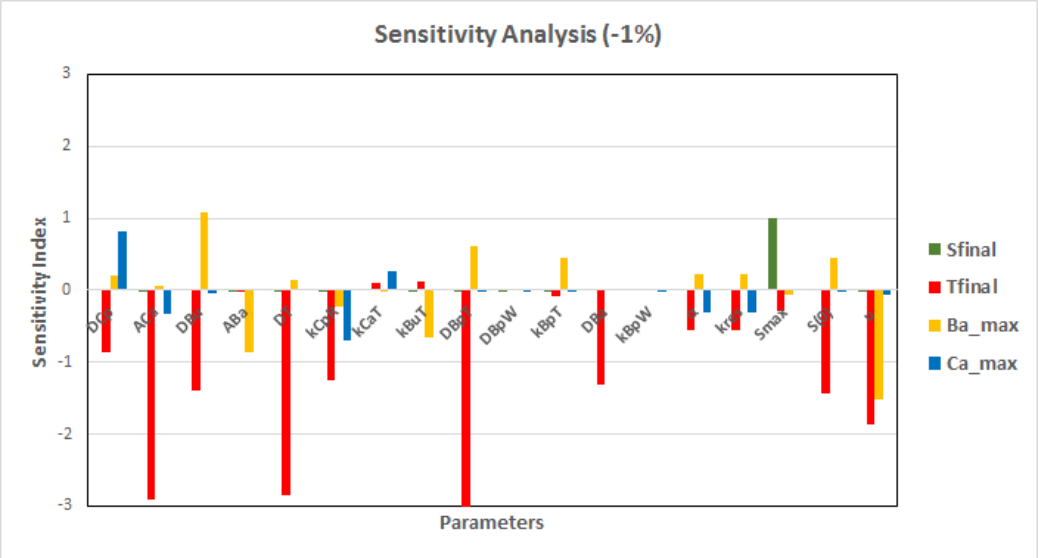

Figure 8. Sensitivity analysis for a 1% decrease in parameters in the main model.

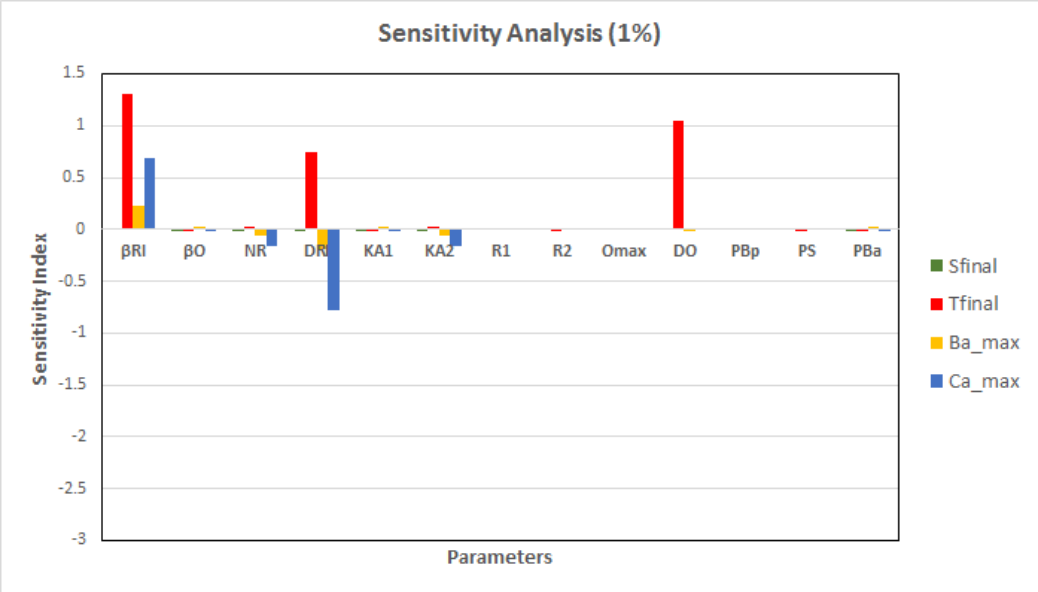

Figure 9. Sensitivity analysis for a 1% increase in parameters in the RANK-RANKL-OPG Pathway.

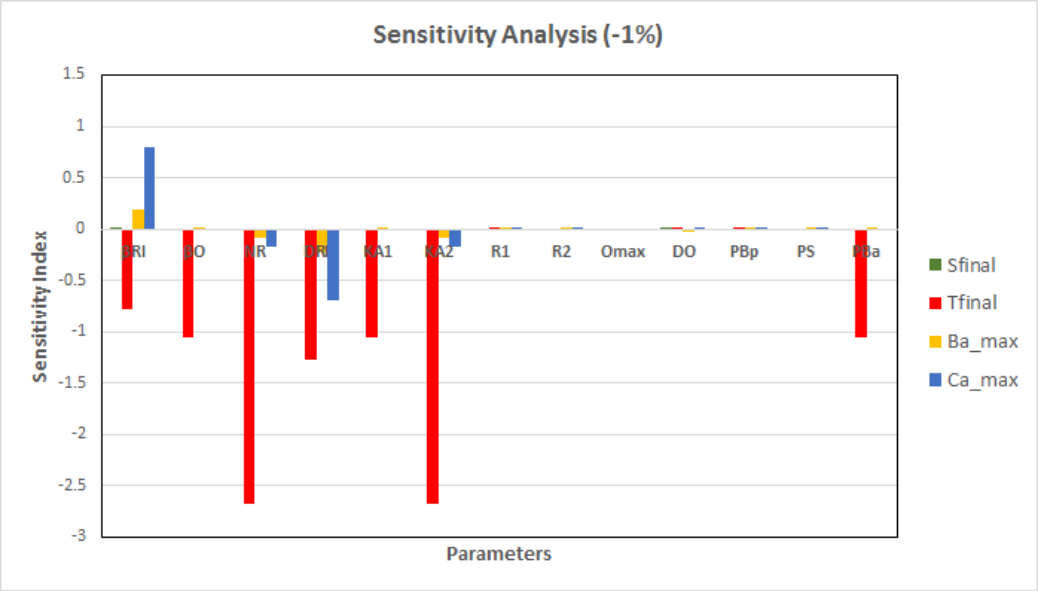

Figure 10. Sensitivity analysis for a 1% decrease in parameters in the RANK-RANKL-OPG Pathway.

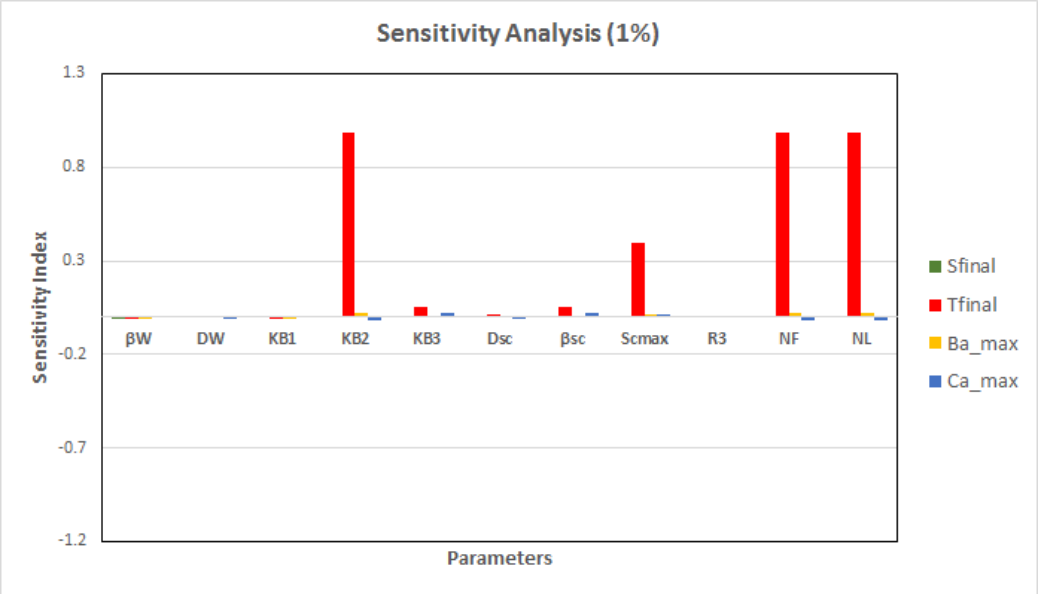

Figure 11. Sensitivity analysis for a 1% increase in parameters in the Wnt Pathway.

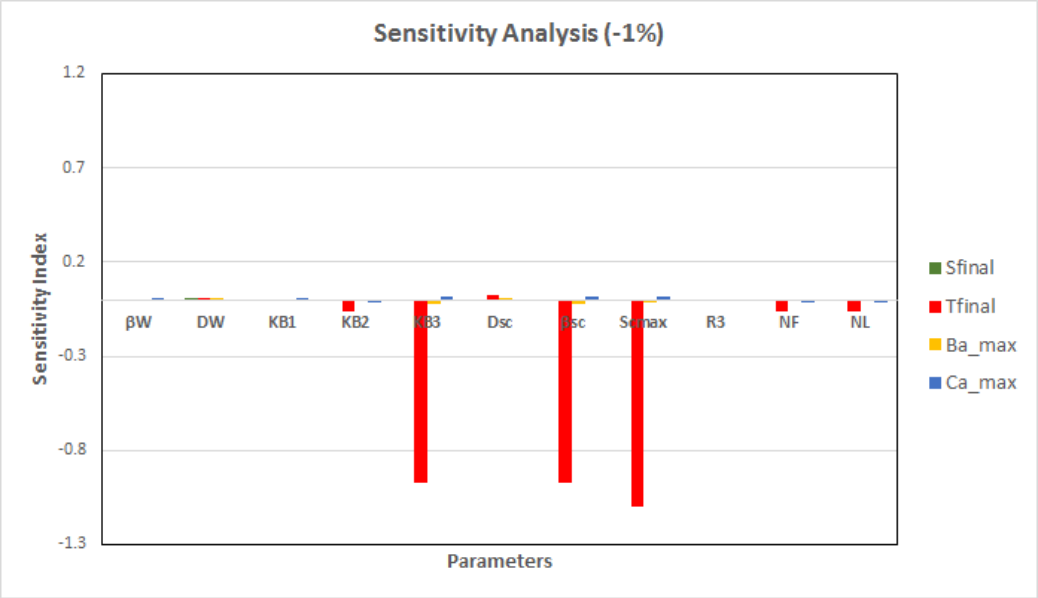

Figure 12. Sensitivity analysis for a 1% decrease in parameters in the Wnt Pathway.

One observation that can be made from our sensitivity analysis (Figures 7-12) is that small changes in parameters will not affect the final osteocyte density, S_{final}. In other words, small changes in parameters will not affect the equilibrium of the system. Most of the parameters did affect the final time to remodel, T_{final}, which allowed us to modify parameters not found in literature (such as the production and degradation rate of sclerostin). Variation in parameters for the Wnt pathway affected the maximum osteoblast density, as expected.

4 Numerical Results using PDE Model

We now study the effects of different sized linear microcracks as found in [32] which gives the mean dimensions of sheet-like, approximately elliptically-shaped microcracks (see Table 4).

4.1 Initial and Boundary Conditions

We use the gaussian equation, once more, to approximate the elliptic shape of the microcracks and give an expression for initial osteocyte density in Equation 95, where ϵ is the proportion of apoptotic osteocytes due to the microcrack size. We give values for epsilon and the longitudinal length, LL, for large, moderate, and small microcracks in Table 5 where dimensions for large and small microcracks are two standard deviations above and below the mean, respectively. Equations 96-98 give the remaining initial conditions and boundary conditions for the system. Note, a single boundary condition is given for the state variables due to the advection term given in Equation 8.

Table 4. Dimensions of Linear Microcracks [32]

Dimension	**Mean**	**Standard Deviation**
Longitudinal Length	$404\mu m$	$145\mu m$
Transverse Length	$97\mu m$	$38\mu m$
Thickness	$9\mu m$	$3\mu m$

Table 5. ϵ and LL Values for Microcrack Sizes

Size	ϵ	LL
Large	0.1	$694\mu m$
Moderate	0.05	$404\mu m$
Small	0.01	$114\mu m$

$$S(x,0) = S_{max} - \epsilon S_{max} e^{-\frac{1}{2}(\frac{x-2000}{LL})^2} \tag{95}$$

$$C_a(x,0) = B_p(x,0) = B_a(x,0) = T(x,0) = 0 \tag{96}$$

$$S(0,t) = S_{max} - \epsilon S_{max} e^{-\frac{1}{2}(\frac{-2000}{LL})^2} \tag{97}$$

$$C_a(0,t) = B_p(0,t) = B_a(0,t) = T(0,t) = 0 \tag{98}$$

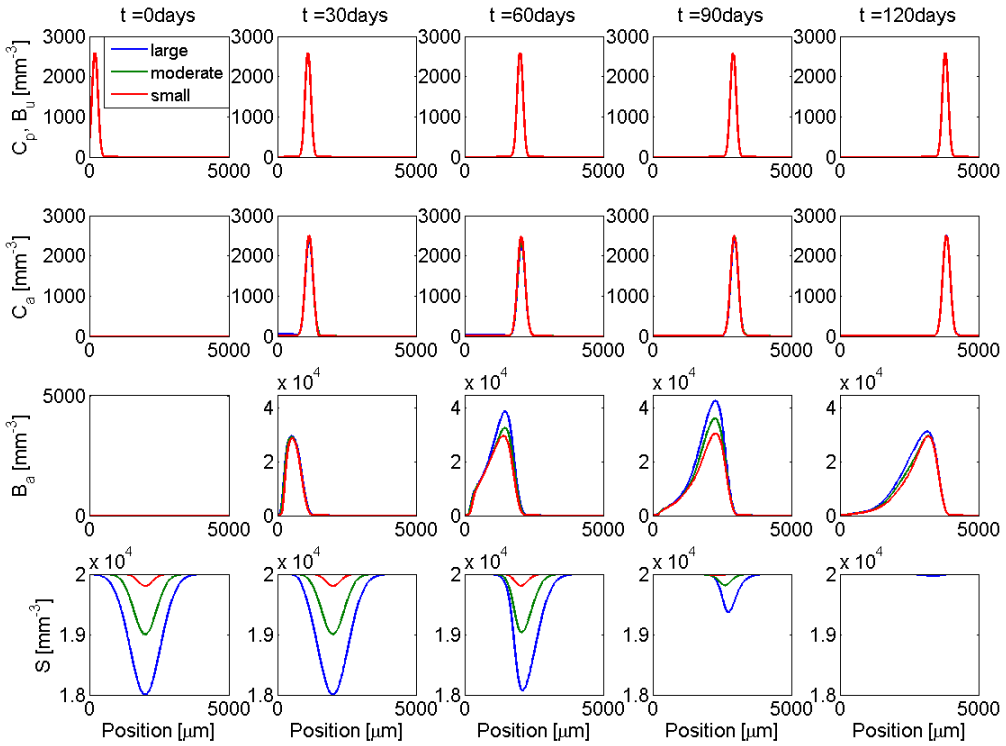

Figure 13. Initiation of the bone remodeling process by large, moderate, and small microcracks.

Figure 13 shows initial large, moderate, and small microcracks (represented by initial concentration of osteocytes). It is observed that all sizes of microcracks are able to initiate the bone remodeling process. Additionally, the figure shows that larger microcracks require longer remodeling time and that greater concentration of osteoblasts are required to remodel the damage.

4.2 Age-related Disorders in Bone

Osteocyte density has been observed to decrease due to age. Many attribute this to a reduction in bone formation, BF within the BMU, while bone resorption, BR,

remains unchanged [42]. Additionally, rapid remodeling, which occurs when the BMU remodels at a much faster pace, is observed in older adults [42]. This phenomena does not allow osteoblast to keep up with the bone resorption done by osteoclast. Both decrease and rapid remodeling also occur in diseases such as osteoporosis and Paget's disease [11]. We run numerical simulations to study both reduced bone formation and rapid remodeling, and compare them to normal remodeling in Figures 14 and 15.

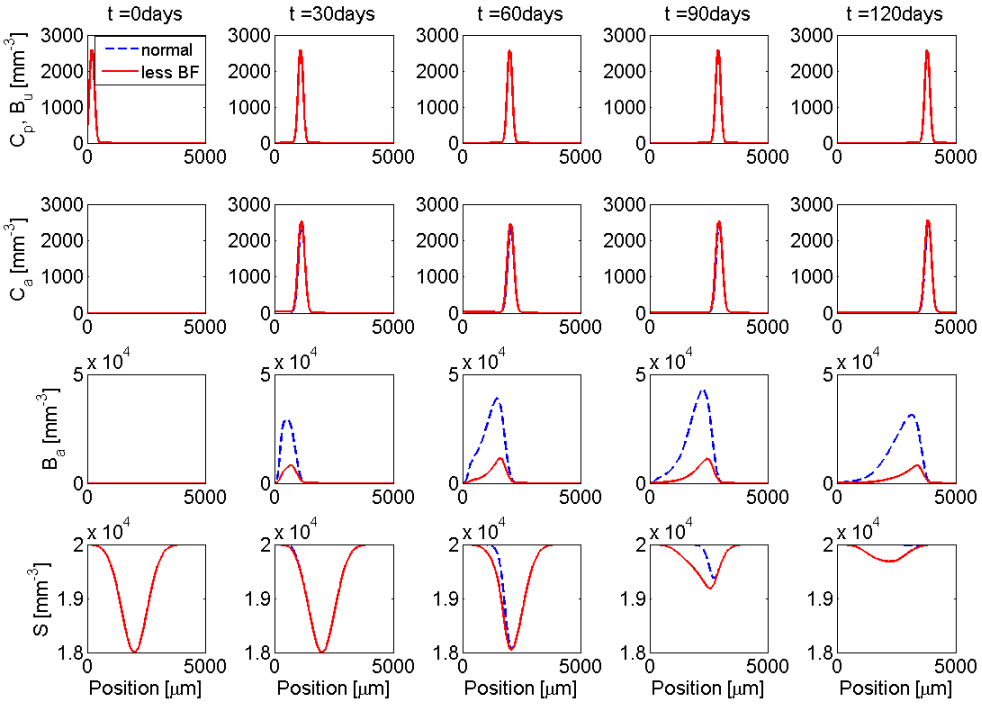

Figure 14. Reduced bone formation in bone compared to normal bone remodeling.

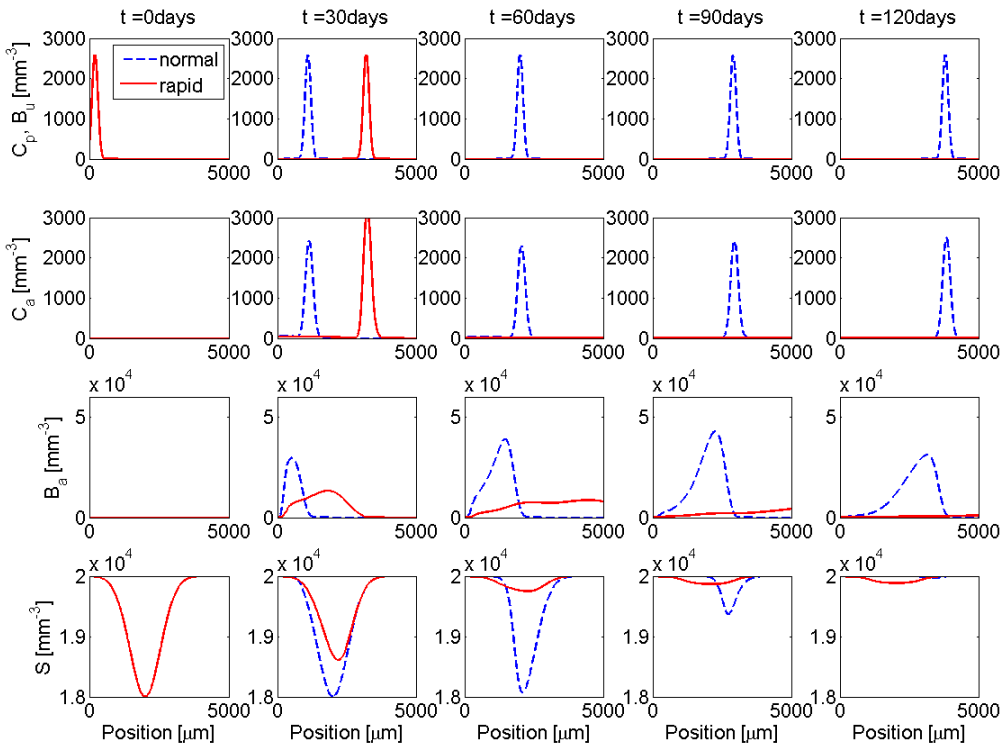

Figure 15. Rapid remodeling compared to normal bone remodeling.

Both age-related disorders show incomplete remodeling. It has been stated in literature that microdamage that goes unrepaired will eventually lead to bone fragility and loss of mechanical properties [43]. A decrease in bone formation caused by a decrease in osteoblast concentration, but no change in osteoclast concentration as is observed in Figure 14. This disorder causes less osteoblast to become embedded in the bone matrix and a lower final osteocyte concentration, thus incomplete remodeling. Rapid remodeling, on the other hand, was obtained by increasing the speed of the BMU. Bone resorption was unchanged and concentration of osteoblast signifi-

cantly decreased. This also cause lower final osteocyte concentration and incomplete remodeling.

4.3 Wnt Canonical Pathway - Therapeutic Targets

The Wnt canonical pathway is known for regulating commitment to the osteoblastic lineage as well as for osteoblastic precursor proliferation and differentiation. Activation of this pathway can result in increased bone mass, where as inhibition can lead to low bone mass and lead to diseases such as osteoporosis. In this section we study three therapeutic targets dealing with the Wnt canonical pathway.

The first therapy $(T-1)$ consisted of increasing the production of Wnt ligands by osteocytes. Figure 32 shows that increasing the production rate is able to increase the final osteocyte density.

The second therapy $(T-2)$ found in literature is the injection of diphenylsulfonyl sulfonamide; this is currently being studied as a means to promote the activation of the Wnt canonical pathway. It does this by inhibiting SFRPs which bind with Wnt ligands, thus increasing the binding affinity of Wnt-Frizzled-LRP. We studied this therapy by decreasing the value of the dissociation constant K_{B2}, which is inversely proportional to the binding affinity of Wnt-Frizzled-LRP. Figure 30 shows that an increase in affinity of Wnt-LRP-Frizzled binding caused by injection of diphenylsulfonyl sulfonamide increases osteoblast cell density, increases the osteocyte density, and decreases the time for remodel.

The third therapy $(T-3)$ that is currently being studied is the injection of antisclerostin antibodies which bind with sclerostin to inhibit sclerostin from binding with LRP. We studied this therapy by decreasing the binding affinity of Sclerostin-LRP binding, which is inversely proportional to the dissociation constant K_{B3}. Figure 31 shows that a decrease in binding affinity of Sclerostin-LRP binding caused by injec-

tion of antisclerostin antibody increases osteoblast cell density, increases the osteocyte density, and decreases the time for remodel.

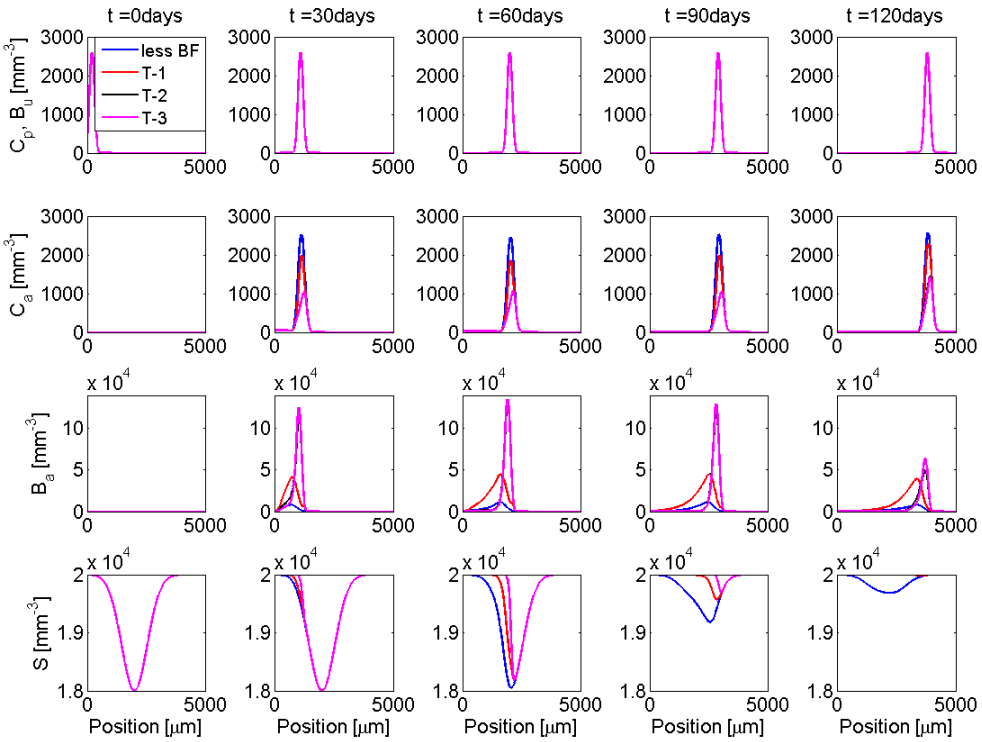

Figure 16. Three potential therapies in the presence of reduced bone formation..

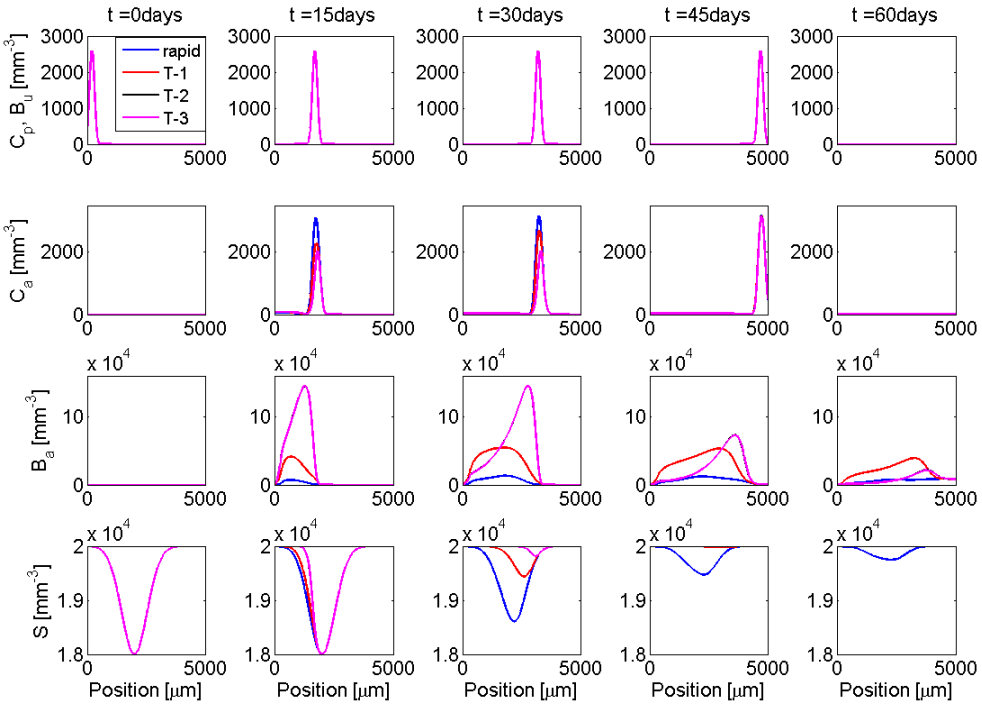

Figure 17. Three potential therapies in the presence of rapid remodeling..

Figures 16 and 17 compares the three therapies when there is decreased bone formation and rapid remodeling, respectively. All three therapies are able to promote bone formation for both disorders, however, therapies 2 and 3 remodel the bone much more quickly.

5 Conclusion and Future Work

In this work, we developed a mathematical model to study the bone remodeling process within the cortical BMU. A major function of bone is to withstand everyday mechanical loading which can cause accumulation of microdamage in the bone matrix. The bone remodeling process is therefore responsible for repairing microdamage and keeping the optimal structure and function of the skeletal system. We study the organization of cells within the BMU, in particular those responsible for sensing damage in the bone matrix, osteocytes, along with two important signaling pathways that are regulated by these cells.

We were able to successfully develop a spatio-temporal model to incorporate the role osteocytes. Our work is the first to explicitly include concentration of ligands and co-receptors in the Wnt canonical pathway using the principle of mass action kinetics which has a potential for targeted therapies that promote bone formation. We performed equilibrium and stability analysis on several simplifications of the model which indicate that the overall system an attracting line of non-isolated equilibria in the $S-$dimension.

We were able to run numerical simulations in MATLAB that studied the initiation of the bone remodeling process through different sized microcracks. Finally, we were able to study biological scenarios for age-related bone disorders and studied therapies to overcome such disorders.

References

[1] L. Arriola and J. M. Hyman. Sensitivity analysis for uncertainty quantification in mathematical models. In *Mathematical and Statistical Estimation Approaches in Epidemiology*, pages 195–247. Springer, 2009.

[2] G. Atkins and D. Findlay. Osteocyte regulation of bone mineral: a little give and take. *Osteoporosis international*, 23(8):2067–2079, 2012.

[3] R. Baron and M. Kneissel. Wnt signaling in bone homeostasis and disease: from human mutations to treatments. *Nature medicine*, 19(2):179–192, 2013.

[4] T. Bellido. Osteocyte-driven bone remodeling. *Calcified tissue international*, 94(1):25–34, 2014.

[5] L. F. Bonewald and S. Dallas. Role of active and latent transforming growth factor β in bone formation. *Journal of cellular biochemistry*, 55(3):350–357, 1994.

[6] L. F. Bonewald and M. L. Johnson. Osteocytes, mechanosensing and wnt signaling. *Bone*, 42(4):606–615, 2008.

[7] P. R. Buenzli, P. Pivonka, B. S. Gardiner, and D. W. Smith. Modelling the anabolic response of bone using a cell population model. *Journal of theoretical biology*, 307:42–52, 2012.

[8] P. R. Buenzli, P. Pivonka, and D. W. Smith. Spatio-temporal structure of cell distribution in cortical bone multicellular units: a mathematical model. *Bone*, 48(4):918–926, 2011.

[9] P. R. Buenzli, P. Pivonka, and D. W. Smith. Bone refilling in cortical basic multicellular units: insights into tetracycline double labelling from a computational model. *Biomechanics and modeling in mechanobiology*, 13(1):185–203, 2014.

[10] P. R. Buenzli and N. A. Sims. Quantifying the osteocyte network in the human skeleton. *Bone*, 75:144–150, 2015.

[11] D. B. Burr. Why does bone remodel, what happens when it doesnt, and how

can we use this to change our therapeutic mindset? *The FASEB Journal*, 31(1_supplement):11–2, 2017.

[12] L. Cardoso, B. C. Herman, O. Verborgt, D. Laudier, R. J. Majeska, and M. B. Schaffler. Osteocyte apoptosis controls activation of intracortical resorption in response to bone fatigue. *Journal of bone and mineral research*, 24(4):597–605, 2009.

[13] X. Feng and J. M. McDonald. Disorders of bone remodeling. *Annual Review of Pathology: Mechanisms of Disease*, 6:121–145, 2011.

[14] J. M. Graham, B. P. Ayati, S. A. Holstein, and J. A. Martin. The role of osteocytes in targeted bone remodeling: a mathematical model. *PloS one*, 8(5):e63884, 2013.

[15] E. M. Greenfield, Y. Bi, and A. Miyauchi. Regulation of osteoclast activity. *Life sciences*, 65(11):1087–1102, 1999.

[16] R. L. Hunter and A. M. Agnew. Intraskeletal variation in human cortical osteocyte lacunar density: Implications for bone quality assessment. *Bone reports*, 5:252–261, 2016.

[17] R. L. Jilka, B. Noble, and R. S. Weinstein. Osteocyte apoptosis. *Bone*, 54(2):264–271, 2013.

[18] P. Juárez and T. A. Guise. Tgf-β in cancer and bone: implications for treatment of bone metastases. *Bone*, 48(1):23–29, 2011.

[19] O. D. Kennedy, D. M. Laudier, R. J. Majeska, H. B. Sun, and M. B. Schaffler. Osteocyte apoptosis is required for production of osteoclastogenic signals following bone fatigue in vivo. *Bone*, 64:132–137, 2014.

[20] J. H. Kim, X. Liu, J. Wang, X. Chen, H. Zhang, S. H. Kim, J. Cui, R. Li, W. Zhang, Y. Kong, et al. Wnt signaling in bone formation and its therapeutic potential for bone diseases. *Therapeutic advances in musculoskeletal disease*,

5(1):13–31, 2013.

[21] Y. Kogan, K. E. Halevi-Tobias, G. Hochman, A. K. Baczmanska, L. Leyns, and Z. Agur. A new validated mathematical model of the wnt signalling pathway predicts effective combinational therapy by sfrp and dkk. *Biochemical Journal*, 444(1):115–125, 2012.

[22] S. V. Komarova, R. J. Smith, S. J. Dixon, S. M. Sims, and L. M. Wahl. Mathematical model predicts a critical role for osteoclast autocrine regulation in the control of bone remodeling. *Bone*, 33(2):206–215, 2003.

[23] I. Kramer, C. Halleux, H. Keller, M. Pegurri, J. H. Gooi, P. B. Weber, J. Q. Feng, L. F. Bonewald, and M. Kneissel. Osteocyte wnt/β-catenin signaling is required for normal bone homeostasis. *Molecular and cellular biology*, 30(12):3071–3085, 2010.

[24] X. Lai, C. Price, S. Modla, W. R. Thompson, J. Caplan, C. B. Kirn-Safran, and L. Wang. The dependences of osteocyte network on bone compartment, age, and disease. *Bone research*, 3:15009, 2015.

[25] D. A. Lauffenburger and J. J. Linderman. *Receptors: models for binding, trafficking, and signaling*. Oxford University Press on Demand, 1996.

[26] V. Lemaire, F. L. Tobin, L. D. Greller, C. R. Cho, and L. J. Suva. Modeling the interactions between osteoblast and osteoclast activities in bone remodeling. *Journal of theoretical biology*, 229(3):293–309, 2004.

[27] S. C. Manolagas. Birth and death of bone cells: basic regulatory mechanisms and implications for the pathogenesis and treatment of osteoporosis 1. *Endocrine reviews*, 21(2):115–137, 2000.

[28] R. Martin. Is all cortical bone remodeling initiated by microdamage? *Bone*, 30(1):8–13, 2002.

[29] M. Mullender, D. Van Der Meer, R. Huiskes, and P. Lips. Osteocyte density

changes in aging and osteoporosis. *Bone*, 18(2):109–113, 1996.

[30] B. S. Noble, N. Peet, H. Y. Stevens, A. Brabbs, J. R. Mosley, G. C. Reilly, J. Reeve, T. M. Skerry, and L. E. Lanyon. Mechanical loading: biphasic osteocyte survival and targeting of osteoclasts for bone destruction in rat cortical bone. *American Journal of Physiology-Cell Physiology*, 284(4):C934–C943, 2003.

[31] F. J. OBrien, O. Brennan, O. D. Kennedy, and T. C. Lee. Microcracks in cortical bone: how do they affect bone biology? *Current osteoporosis reports*, 3(2):39–45, 2005.

[32] F. J. O'BRIEN, D. Taylor, G. Dickson, and T. C. Lee. Visualisation of three-dimensional microcracks in compact bone. *The Journal of Anatomy*, 197(3):413–420, 2000.

[33] F. J. OBrien, D. Taylor, and T. C. Lee. The effect of bone microstructure on the initiation and growth of microcracks. *Journal of Orthopaedic Research*, 23(2):475–480, 2005.

[34] A. Parfitt. Osteonal and hemi-osteonal remodeling: the spatial and temporal framework for signal traffic in adult human bone. *Journal of cellular biochemistry*, 55(3):273–286, 1994.

[35] A. Parfitt. Targeted and nontargeted bone remodeling: relationship to basic multicellular unit origination and progression. *Bone*, 30(1):5–7, 2002.

[36] P. Pivonka and S. V. Komarova. Mathematical modeling in bone biology: From intracellular signaling to tissue mechanics. *Bone*, 47(2):181–189, 2010.

[37] P. Pivonka, J. Zimak, D. W. Smith, B. S. Gardiner, C. R. Dunstan, N. A. Sims, T. J. Martin, and G. R. Mundy. Model structure and control of bone remodeling: a theoretical study. *Bone*, 43(2):249–263, 2008.

[38] Q.-H. Qin and Y.-N. Wang. A mathematical model of cortical bone remodeling at cellular level under mechanical stimulus. *Acta Mechanica Sinica*, 28(6):1678–

1692, 2012.

[39] J.-Y. Rho, L. Kuhn-Spearing, and P. Zioupos. Mechanical properties and the hierarchical structure of bone. *Medical engineering and physics*, 20(2):92–102, 1998.

[40] M. D. Ryser, N. Nigam, and S. V. Komarova. Mathematical modeling of spatio-temporal dynamics of a single bone multicellular unit. *Journal of bone and mineral research*, 24(5):860–870, 2009.

[41] A. Saltelli, M. Ratto, T. Andres, F. Campolongo, J. Cariboni, D. Gatelli, M. Saisana, and S. Tarantola. *Global sensitivity analysis: the primer*. John Wiley & Sons, 2008.

[42] E. Seeman. Structural basis of growth-related gain and age-related loss of bone strength proceedings of a satellite symposium held on the occasion of the eular congress, paris, france, june 13, 2008. *Rheumatology*, 47(suppl_4):iv2–iv8, 2008.

[43] Z. Seref-Ferlengez, O. D. Kennedy, and M. B. Schaffler. Bone microdamage, remodeling and bone fragility: how much damage is too much damage [quest]. *BoneKEy reports*, 4, 2015.

[44] D. Vashishth, G. Gibson, J. Kimura, M. Schaffler, and D. Fyhrie. Determination of bone volume by osteocyte population. *The Anatomical Record*, 267(4):292–295, 2002.

[45] D. Vashishth, O. Verborgt, G. Divine, M. Schaffler, and D. Fyhrie. Decline in osteocyte lacunar density in human cortical bone is associated with accumulation of microcracks with age. *Bone*, 26(4):375–380, 2000.

[46] J. Xiong and C. A. O'Brien. Osteocyte rankl: new insights into the control of bone remodeling. *Journal of Bone and Mineral Research*, 27(3):499–505, 2012.

[47] M. P. Yavropoulou, A. Michopoulos, and J. G. Yovos. Pth and pthr1 in osteocytes. new insights into old partners. *Hormones (Athens, Greece)*, 16(2):150–160,

2017.

Appendix A - Parameter Values

Table 6. Parameter Values - main PDE model

Symbol	Description	Value	Reference
D_{C_p}	maximum differentiation rate of C_p	41.26 day^{-1}	[9]
A_{C_a}	maximum apoptosis rate of C_a	2.82 day^{-1}	[9]
$D^T_{B_u}$	maximum differentiation rate of B_u due to TGF-β	20.2675 day^{-1}	
$D^W_{B_u}$	maximum differentiation rate of B_u due to Wnt Pathway	30.40125 day^{-1}	
$k^T_{B_u}$	dissociation binding constant for $TGF-\beta$ binding on B_u	339.2 mm^{-3}	[9]
$k^W_{B_u}$	dissociation binding constant for Wnt binding on B_u	1.204x10^6 mm^{-3}	[7]
$D^T_{B_p}$	maximum differentiation rate of B_p due to $TGF-\beta$	0.05 day^{-1}	
$D^W_{B_p}$	maximum differentiation rate of B_p due to Wnt Pathway	0.5 day^{-1}	
$k^T_{B_p}$	dissociation binding constant for $TGF-\beta$ binding on B_p	105.6 mm^{-3}	[9]
$k^W_{B_p}$	dissociation binding constant for Wnt binding on B_p	1.204x10^6 mm^{-3}	[7]
$k^R_{C_p}$	dissociation binding constant for RANKL binding on C_p	1.0025x10^7 mm^{-3}	[9]
$k^T_{C_a}$	dissociation binding constant for $TGF-beta$ binding on C_a	339.2 mm^{-3}	[9]
α	concentration of $TGF-\beta$ found in the bone matrix	3946 mm^{-3}	[9]
k_{res}	bone volume resorbed per unit time by a single osteoclast	9.425x10^{-6} mm^3/day	[9]
D_{B_a}	rate at which osteoblasts become embedded in the bone matrix	0.1 day^{-1}	
A_{B_a}	apoptosis rate of B_a	0.1 day^{-1}	
D_T	degradation rate of $TGF-\beta$	0.5 day^{-1}	[9]
S_{max}	maximum osteocyte density per unit of volume	20000 mm^{-3}	[10]
u	average speed of the BMU's progression	0.03 mm/day	[34]
p_{max}	maximum concentration of B_u or C_p at the tip of the capilary	2589 mm^{-3}	[9]
b	initial position of the tip of the capillary	0.2 mm	
c	width of the gaussian curve	0.1 mm	[34]

Table 7. Parameter Values - RANK-RANKL-OPG Pathway

Symbol	Description	Value	Reference
β_{Rl}	production rate of RANKL	3.48377x10^{6}day^{-1}	
β_O	production rate of OPG	326305 day^{-1}	[9]
N_R	number of RANK receptors expressed on C_p	2326	[9]
$\hat{D}_{Rl}$	degradation rate of RANKL	10.13 day^{-1}	[9]
K_{A_1}	association binding constant for RANKL-OPG	1.66058x10^{-9} mm^3	[9]
K_{A_2}	association binding constant for RANK-RANKL	5.6655x10^{-8} mm^3	[9]
R_1	maximum number of RANKL on the surface of B_p	2.7x10^6	[9]
R_2	maximum concentration of RANKL produced per S	2.7x10^6	
O_{max}	maximum possible OPG concentration	1.205x10^{14} mm^{-3}	[9]
$\hat{D}_O$	degradation rate of OPG	0.35 day^{-1}	[9]
π_{PTH,B_p}	activation parameter for RANKL related to PTH on B_p	0.019	[9]
$\pi_{PTH,S}$	activation parameter for RANKL related to PTH on S	0.019	
π_{PTH,B_a}	repressions parameter for OPG related to PTH on B_a	0.0711	[9]

Table 8. Parameter Values - Wnt Canonical Pathway

Symbol	**Description**	**Value**	**Reference**
β_W	production rate of Wnt	10^7 day^{-1}	[7]
$\hat{D}_W$	degradation rate of Wnt	2 day^{-1}	[7]
K_{B_1}	association binding constant for Wnt-Frizzled	3.8x10^{-8} mm^3	[21]
K_{B_2}	association binding constant for Frizzled-LRP	1.3393x10^{-5} mm^3	[21]
K_{B_3}	association binding constant for LRP-sclerostin	4.93x10^{-7} mm^3	[21]
R_3	maximum concentration of Wnt produced per S	2.7x10^6	
β_{Sc}	production rate of sclerostin	3.26305x10^8 day^{-1}	
Sc_{max}	maximum possible sclerostin concentration	6.5261x10^{1}2 mm^{-3}	
$\hat{D}_{Sc}$	degradation rate of sclerostin	0.35 day^{-1}	
N_F	number of Frizzled receptors expressed on B_p	30	[21]
N_L	number of LRP receptors expressed on B_p	4000	[21]

Appendix B - Additional Sensitivity Analysis

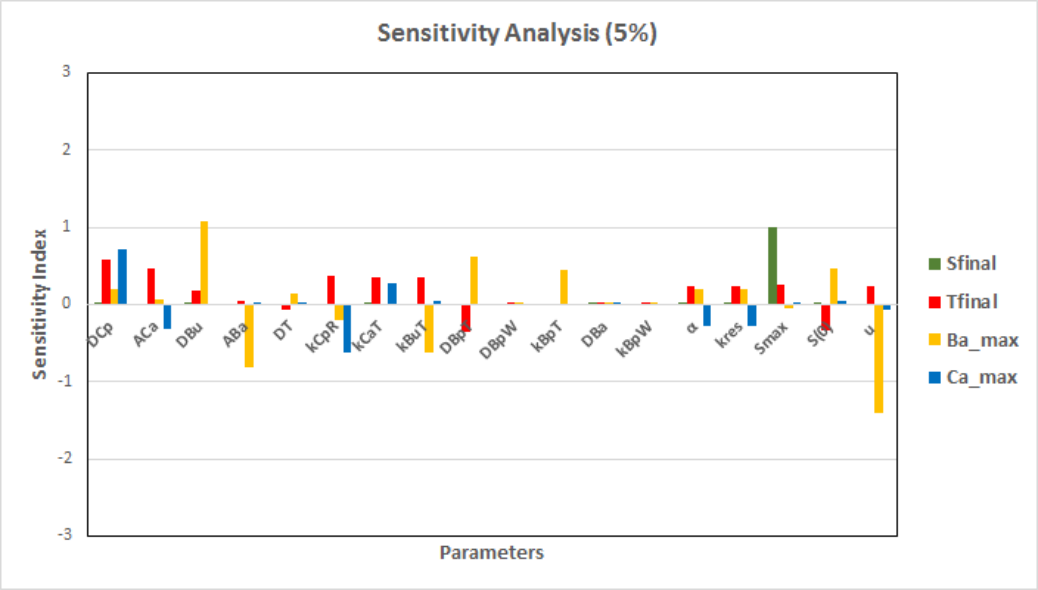

Figure 18. Sensitivity analysis for a 5% increase in parameters in the main model.

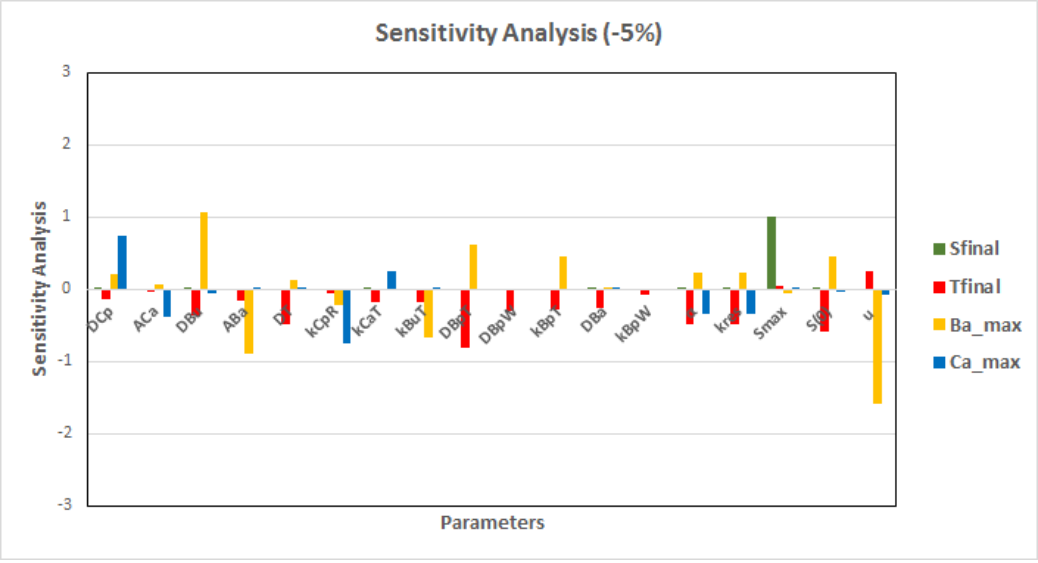

Figure 19. Sensitivity analysis for a 5% decrease in parameters in the main model.

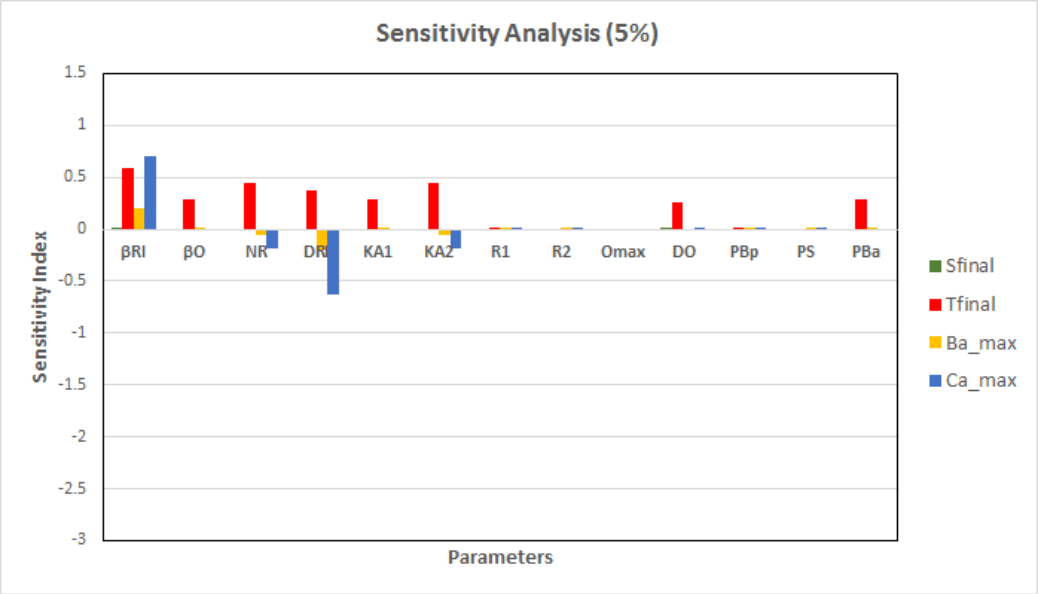

Figure 20. Sensitivity analysis for a 5% increase in parameters in the RANK-RANKL-OPG Pathway.

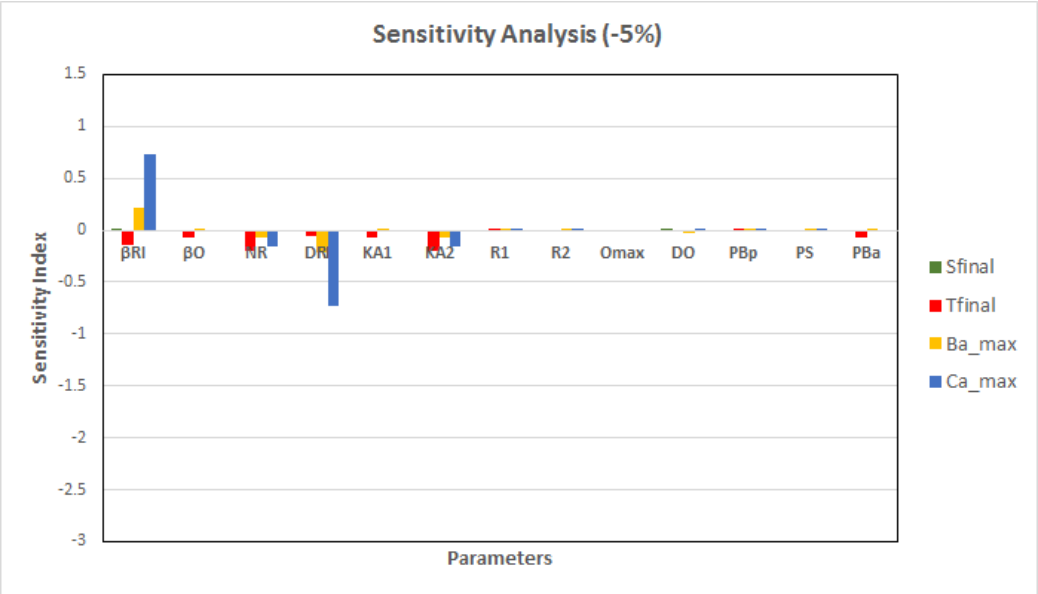

Figure 21. Sensitivity analysis for a 5% decrease in parameters in the RANK-RANKL-OPG Pathway.

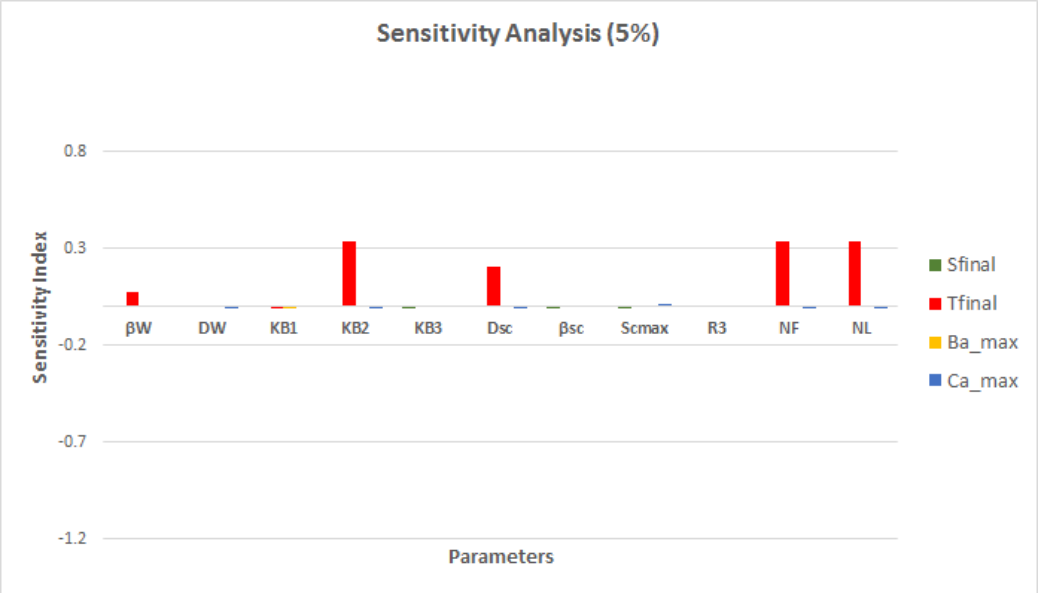

Figure 22. Sensitivity analysis for a 5% increase in parameters in the Wnt Pathway.

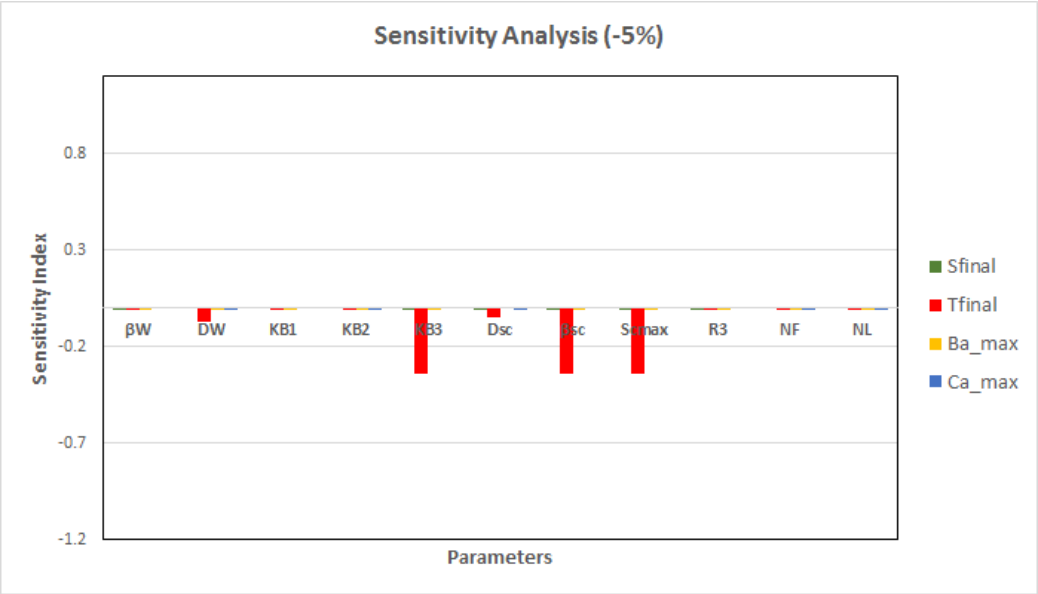

Figure 23. Sensitivity analysis for a 5% decrease in parameters in the Wnt Pathway.

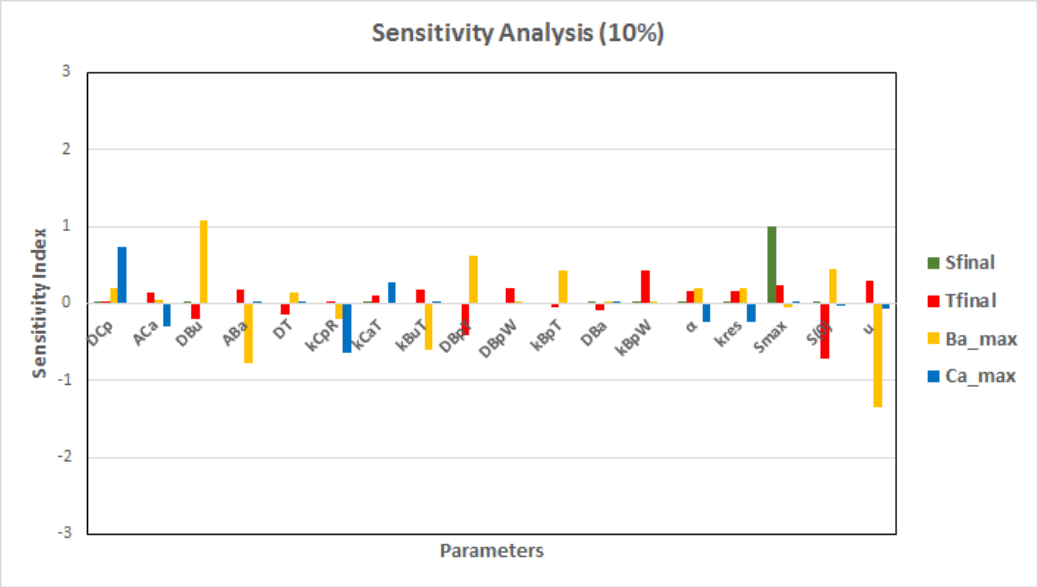

Figure 24. Sensitivity analysis for a 10% increase in parameters in the main model.

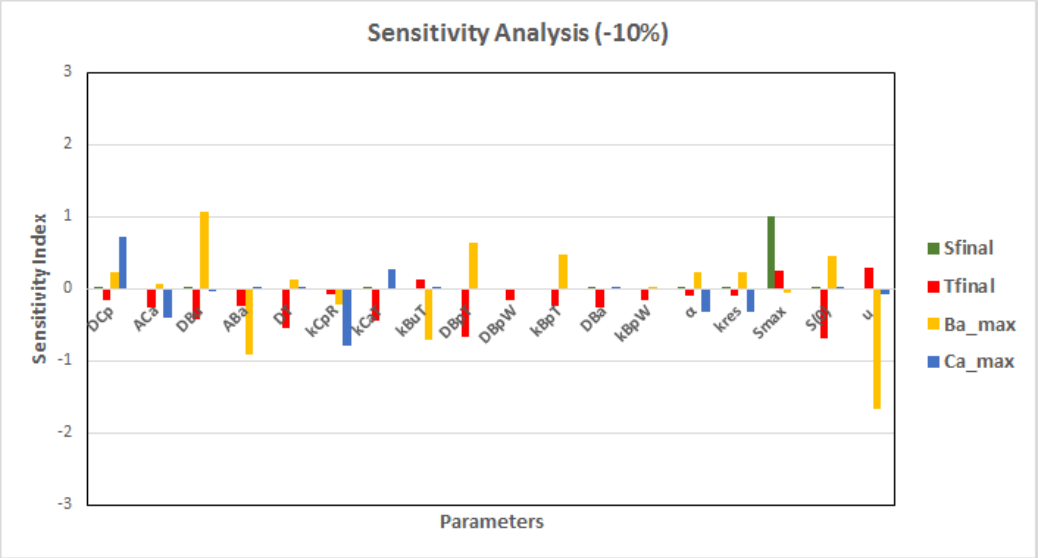

Figure 25. Sensitivity analysis for a 10% decrease in parameters in the main model.

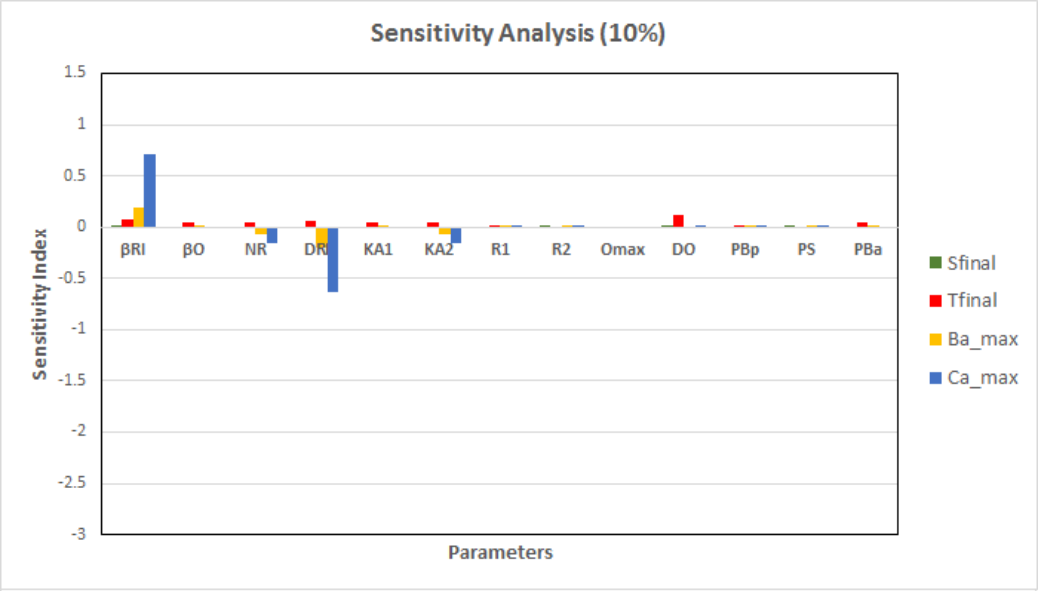

Figure 26. Sensitivity analysis for a 10% increase in parameters in the RANK-RANKL-OPG Pathway.

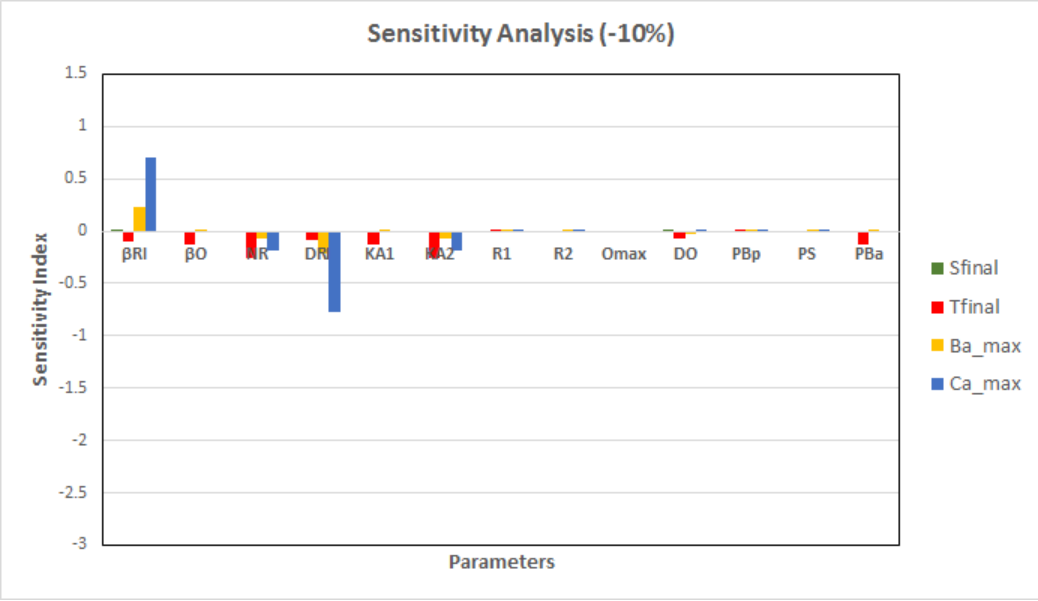

Figure 27. Sensitivity analysis for a 10% decrease in parameters in the RANK-RANKL-OPG Pathway.

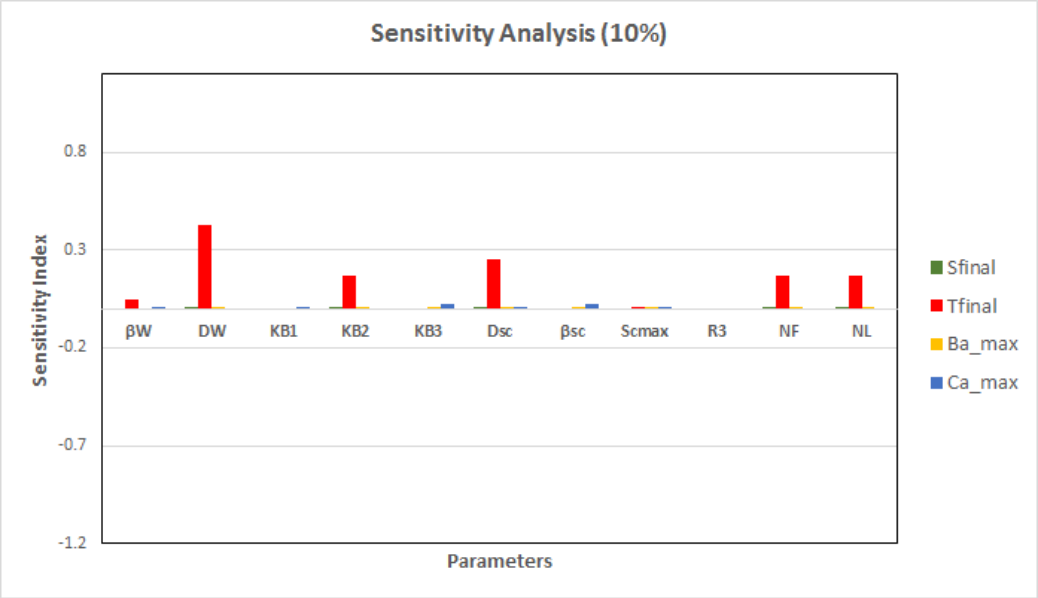

Figure 28. Sensitivity analysis for a 10% increase in parameters in the Wnt Pathway.

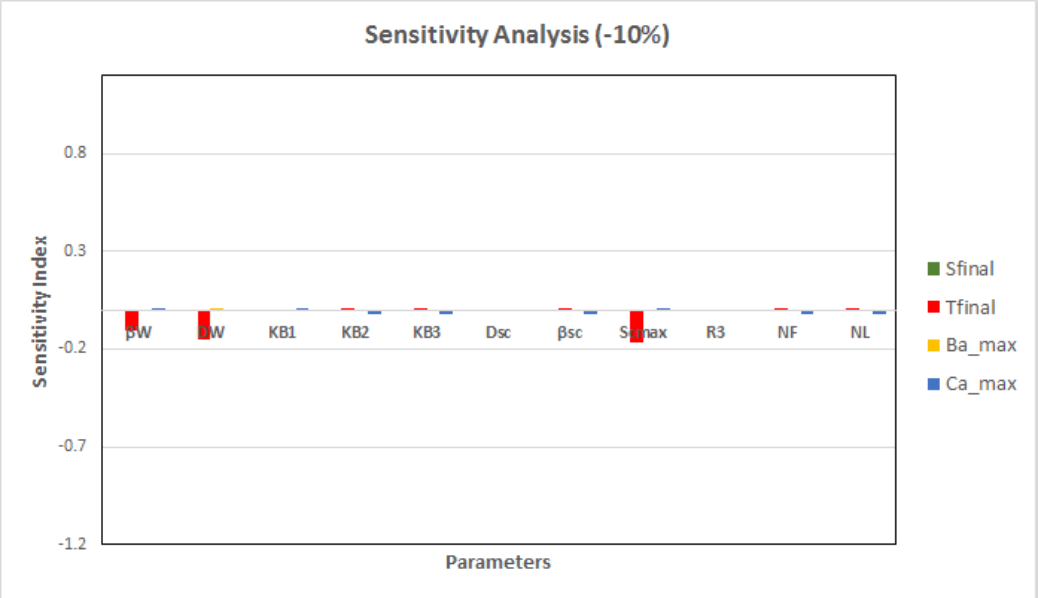

Figure 29. Sensitivity analysis for a 10% decrease in parameters in the Wnt Pathway.

Appendix C - Additional Figures

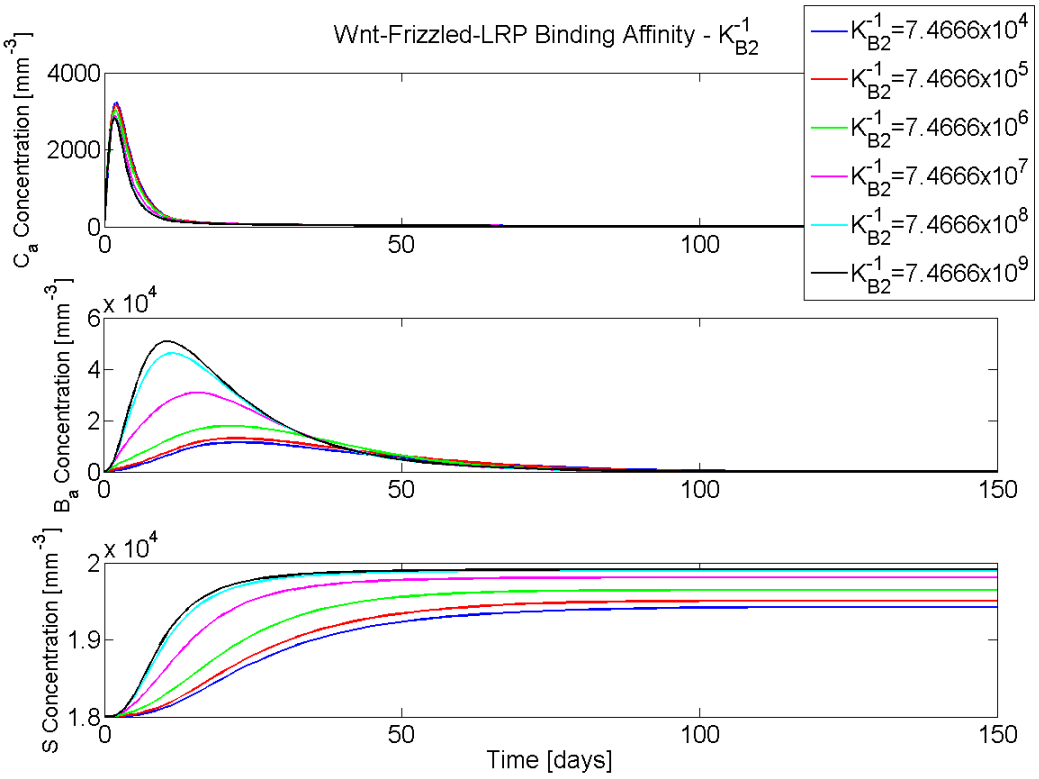

Figure 30. Therapeutic Target: Inject diphenylsulfonyl sulfonamide which inhibits SFRP binding with Wnt and promotes Wnt-LRP-Frizzled binding.

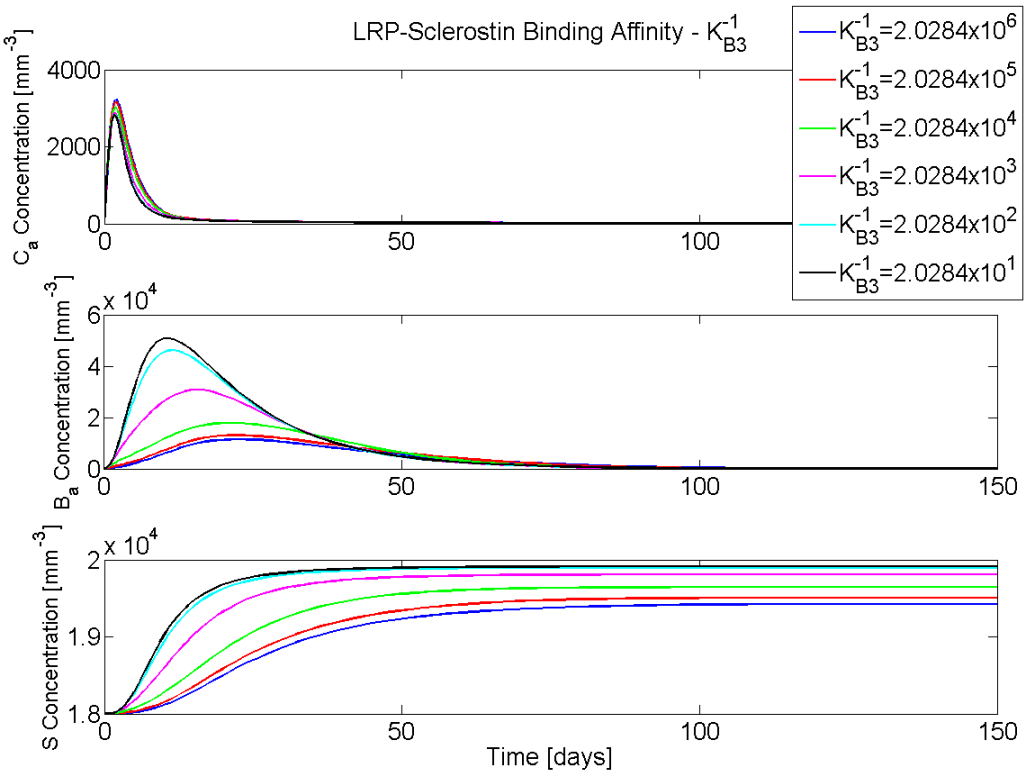

Figure 31. Therapeutic Target: Inject antisclerostin antibody which binds with sclerostin and inhibits Sclerostin-LRP binding.

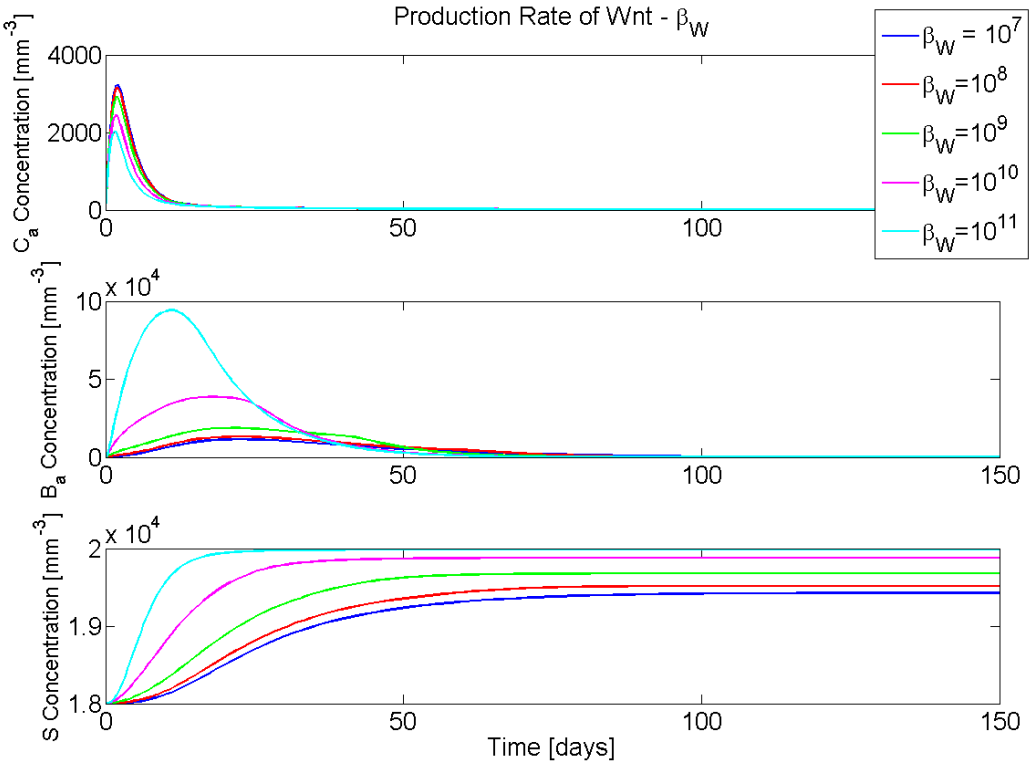

Figure 32. Increase production of Wnt ligand by osteocytes.

Biographical Statement

Iris Lizeth Alvarado, born May 22, 1989 in Mission, Texas, graduated Magna Cum Laude with a Bachelor of Science in Mechanical Engineering and Mathematics from the University of Texas-Pan American (UTPA) in 2011. She went on to receive her Master's Degree in Mechanical Engineering from UTPA in 2012, before deciding to pursue a PhD in Mathematics at the University of Texas at Arlington (UTA).

Iris began the Doctoral Program in January 2013, where she received funding as a Graduate Teaching Assistant and had the opportunity to teach various courses ranging from Fundamentals of Algebra to Calculus 2. She received various fellowships during her time at UTA such as the NSF GK-12 MAVS, MAVS Bridge, GAANN, and the 2018 Summer Dissertation Fellowships. She obtained the GAANN Peer Mentor Award in 2016, as well as the Outstanding Graduate Teaching Award in 2018. During her time at UTA, she conducted research in Mathematical Biology under the advisement of Dr. Hristo Kojouharov.

After Iris graduates as a Doctor of Philosophy in Mathematics in August 2018, she plans to pursue her passion of sharing the beauty, logic, and structure of mathematics through teaching.